105. **Pritham, E. J., C. Feschotte, and S. R. Wessler.** 2005. Unexpected diversity and differential success of DNA transposons in four species of entamoeba protozoans. *Mol. Biol. Evol.* 22:1751–1763.
106. **Purdy, J. E., L. T. Pho, B. J. Mann, and W. A. Petri, Jr.** 1996. Upstream regulatory elements controlling expression of the *Entamoeba histolytica* lectin. *Mol. Biochem. Parasitol.* 78:91–103.
107. **Que, X., and S. L. Reed.** 2000. Cysteine proteinases and the pathogenesis of amebiasis. *Clin. Microbiol. Rev.* 13:196–206.
108. **Quon, D. V., M. G. Delgadillo, and P. J. Johnson.** 1996. Transcription in the early diverging eukaryote *Trichomonas vaginalis*: an unusual RNA polymerase II and alpha-amanitin-resistant transcription of protein-coding genes. *J. Mol. Evol.* 43:253–262.
109. **Ramakrishnan, G., C. A. Gilchrist, H. Musa, M. S. Torok, P. A. Grant, B. J. Mann, and W. A. Petri, Jr.** 2004. Histone acetyltransferases and deacetylase in *Entamoeba histolytica*. *Mol. Biochem. Parasitol.* 138:205–216.
110. **Ramos, M. A., G. C. Mercado, L. M. Salgado, R. Sanchez-Lopez, R. P. Stock, P. M. Lizardi, and A. Alagón.** 1997. *Entamoeba histolytica* contains a gene encoding a homologue to the 54 kDa subunit of the signal recognition particle. *Mol. Biochem. Parasitol.* 88:225–235.
111. **Reed, S. L., W. E. Keene, and J. H. McKerrow.** 1989. Thiol proteinase expression and pathogenicity of *Entamoeba histolytica*. *J. Clin. Microbiol.* 27:2772–2777.
112. **Rivera, W. L., S. R. Santos, and H. Kanbara.** 2006. Prevalence and genetic diversity of *Entamoeba histolytica* in an institution for the mentally retarded in the Philippines. *Parasitol. Res.* 98:106–110.
113. **Rojas, R., T. van Vlijmen, G. A. Mardones, Y. Prabhu, A. L. Rojas, S. Mohammed, A. J. Heck, G. Raposo, P. van der Sluijs, J. S. Bonifacino.** 2008. Regulation of retromer recruitment to endosomes by sequential action of Rab5 and Rab7. *J. Cell Biol.* 183:513–526.
114. **Saito-Nakano, Y., B. N. Mitra, K. Nakada-Tsukui, D. Sato, and T. Nozaki.** 2007. Two Rab7 isotypes, EhRab7A and EhRab7B, play distinct roles in biogenesis of lysosomes and phagosomes in the enteric protozoan parasite *Entamoeba histolytica*. *Cell Microbiol.* 9:1796–1808.
115. **Saito-Nakano, Y., B. J. Loftus, N. Hall, and T. Nozaki.** 2005. The diversity of Rab GTPases in *Entamoeba histolytica*. *Exp. Parasitol.* 110:244–252.
116. **Saito-Nakano, Y., T. Yasuda, K. Nakada-Tsukui, M. Leippe, and T. Nozaki.** 2004. Rab5-associated vacuoles play a unique role in phagocytosis of the enteric protozoan parasite *Entamoeba histolytica*. *J. Biol. Chem.* 279:49497–49507.
117. **Sajid, M., and J. H. McKerrow.** 2002. Cysteine proteases of parasitic organisms. *Mol. Biochem. Parasitol.* 120:1–21.
118. **Sanchez, L., V. Enea, and D. Eichinger.** 1994. Identification of a developmentally regulated transcript expressed during encystation of *Entamoeba invadens*. *Mol. Biochem. Parasitol.* 67:125–135.
119. **Schulte, W., and H. Scholze.** 1989. Action of the major protease from *Entamoeba histolytica* on proteins of the extracellular matrix. *J. Protozool.* 6:538–543.
120. **Shah, P. H., R. C. MacFarlane, D. Bhattacharya, J. C. Matese, J. Demeter, S. E. Stroup, and U. Singh.** 2005. Comparative genomic hybridizations of *Entamoeba* strains reveal unique genetic fingerprints that correlate with virulence. *Eukaryot. Cell* 4:504–515.
121. **Sharma, R., A. Bagchi, A. Bhattacharya, and S. Bhattacharya.** 2001. Characterization of a retrotransposon-like element from *Entamoeba histolytica*. *Mol. Biochem. Parasitol.* 116: 45–53.
122. **Shire, A. M., and J. P. Ackers.** 2007. SINE elements of *Entamoeba dispar*. *Mol. Biochem. Parasitol.* 152:47–52.
123. **Singh, U., C. A. Gilchrist, J. M. Schaenman, J. B. Rogers, J. W. Hockensmith, B. J. Mann, and W. A. Petri.** 2002. Context-dependent roles of the *Entamoeba histolytica* core promoter element GAAC in transcriptional activation and protein complex assembly. *Mol. Biochem. Parasitol.* 120: 107–116.
124. **Singh, U., and J. B. Rogers.** 1998. The novel core promoter element GAAC in the hgl5 gene of *Entamoeba histolytica* is able to direct a transcription start site independent of TATA or initiator regions. *J. Biol. Chem.* 273:21663–21668.
125. **Singh, U., J. B. Rogers, B. J. Mann, and W. A. Petri, Jr.** 1997. Transcription initiation is controlled by three core promoter elements in the hgl5 gene of the protozoan parasite *Entamoeba histolytica*. *Proc. Natl. Acad. Sci. USA* 94:8812–8817.
126. **Smith, M., V. Bhaskar, J. Fernandez, and A. J. Courey.** 2004. *Drosophila* Ulp1, a nuclear pore-associated SUMO protease, prevents accumulation of cytoplasmic SUMO conjugates. *J. Biol. Chem.* 279:43805–43814.
127. **Stanley, S. L. Jr., T. Zhang, D. Rubin, and E. Li.** 1995. Role of the *Entamoeba histolytica* cysteine proteinase in amebic liver abscess formation in severe combined immunodeficient mice. *Infect. Immun.* 63:1587–1590.
128. **Stauffer, W., and J. I. Ravdin.** 2003. *Entamoeba histolytica*: an update. *Curr. Opin. Infect. Dis.* 16:479–485.
129. **Suzuki, J., S. Kobayashi, I. Iku, R. Murata, Y. Yanagawa, and T. Takeuchi.** 2008. Seroprevalence of *Entamoeba histolytica* infection in female outpatients at a sexually transmitted disease sentinel clinic in Tokyo, Japan. *Jpn. J. Infect. Dis.* 61:175–178.
130. **Takai, Y., T. Sasaki, and T. Matozaki.** 2001. Small GTP-binding proteins. *Physiol. Rev.* 81:153–208.
131. **Tanyuksel, M., M. Ulukanligil, Z. Guclu, E. Araz, O. Koru, and W. A. Petri, Jr.** 2007. Two cases of rarely recognized infection with *Entamoeba moshkovskii*. *Am. J. Trop. Med. Hyg.* 76:723–724.
132. **Tanyuksel, M., and W. A. Petri, Jr.** 2003. Laboratory diagnosis of amebiasis. *Clin. Microbiol. Rev.* 16:713–729.
133. **Tazreiter, M., D. Leitsch, E. Hatzenbichler, G. E. Mair-Scorpio, R. Steinborn, M. Schreiber, and M. Duchêne.** 2008. *Entamoeba histolytica*: response of the parasite to metronidazole challenge on the levels of mRNA and protein expression. *Exp. Parasitol.* 120:403–410.
134. **Tillack, M., L. Biller, H. Irmer, M. Freitas, M. A. Gomes, E. Tannich, and I. Bruchhaus.** 2007. The *Entamoeba histolytica* genome: primary structure and expression of proteolytic enzymes. *BMC Genomics* 8:170.
135. **Tillack, M., N. Nowak, H. Lotter, R. Bracha, D. Mirelman, E. Tannich, and I. Bruchhaus.** 2006. Increased expression of the major cysteine proteinases by stable episomal transfection underlines the important role of EhCP5 for the pathogenicity of *Entamoeba histolytica*. *Mol. Biochem. Parasitol.* 149:58–64.
136. **Tokoro, M., T. Asai, S. Kobayashi, T. Takeuchi, and T. Nozaki.** 2003. Identification and characterization of two isoenzymes of methionine gamma-lyase from *Entamoeba histolytica*: a key enzyme of sulfur-amino acid degradation in an anaerobic parasitic protist that lacks forward and reverse trans-sulfuration pathways. *J. Biol. Chem.* 278:42717–42727.
137. **Tolstrup, J., E. Krause, E. Tannich, and I. Bruchhaus.** 2007. Proteomic analysis of *Entamoeba histolytica*. *Parasitology* 34: 289–298.
138. **Touz, M. C., M. J. Nores, I. Slavin, C. Carmona, J. T. Conrad, M. R. Mowatt, T. E. Nash, C. E. Coronel, and**

H. D. Luján. 2002. The activity of a developmentally regulated cysteine proteinase is required for cyst wall formation in the primitive eukaryote *Giardia lamblia*. *J. Biol. Chem.* **277**:8474–8481.

139. **Tshalaia, L. E.** 1941. On a species of *Entamoeba* detected in sewage effluents. *Med. Parazit.* (Moscow) **10**:244–252.
140. **Vanacova, S., D. R. Liston, J. Tachezy, and P. J. Johnson.** 2003. Molecular biology of the amitochondriate parasites, *Giardia intestinalis*, *Entamoeba histolytica* and *Trichomonas vaginalis*. *Int. J. Parasitol.* **33**:235–255.
141. **Vargas, M., and C. H. Gonzalez-de la Rosa.** 2007. Structural and functional organization of the RhoGEF proteins from *Entamoeba histolytica*, p. 339–359. *In* Terrazes, L. I. (ed.), *Advances in the Immunobiology of Parasitic Diseases*, Research Signpost, Kerala, India.
142. **Vayssié, L., M. Vargas, C. Weber, and N. Guillén.** 2004. Double-stranded RNA mediates homology-dependent gene silencing of gamma-tubulin in the human parasite *Entamoeba histolytica*. *Mol. Biochem. Parasitol.* **138**:21–28.
143. **Vicente, J. B., G. M. Ehrenkaufer, L. M. Saraiva, M. Teixeira, and U. Singh.** 2009. *Entamoeba histolytica* modulates a complex repertoire of novel genes in response to oxidative and nitrosative stresses: implications for amebic pathogenesis. *Cell Microbiol.* **11**:51–69.
144. **Weber, C., L. A. Marchat, N. Guillen, and C. López-Camarillo.** 2009. Effects of DNA damage induced by UV irradiation on gene expression in the protozoan parasite *Entamoeba histolytica*. *Mol. Biochem. Parasitol.* **164**:165–169.
145. **Weber, C., G. Guigon, C. Bouchier, L. Frangeul, S. Moreira, O. Sismeiro, C. Gouyette, D. Mirelman, J. Y. Coppee, and N. Guillén.** 2006. Stress by heat shock induces massive down regulation of genes and allows differential allelic expression of the Gal/GalNAc lectin in *Entamoeba histolytica*. *Eukaryot. Cell* **5**: 871–875.
146. **Welter, B. H., and L. A. Temesvari.** 2009. Overexpression of a mutant form of EhRabA, a unique Rab GTPase of *Entamoeba histolytica*, alters endoplasmic reticulum morphology and localization of the Gal/GalNAc adherence lectin. *Eukaryot. Cell* **8**:1014–1026.
147. **Welter, B. H., R. R. Powell, M. Leo, C. M. Smith, and L. A. Temesvari.** 2005. A unique Rab GTPase, EhRabA, is involved in motility and polarization of *Entamoeba histolytica* cells. *Mol. Biochem. Parasitol.* **140**:161–173.
148. **Willhoeft, U., and E. Tannich.** 1999. The electrophoretic karyotype of *Entamoeba histolytica*. *Mol. Biochem. Parasitol.* **99**:41–53.
149. **Yoshimori, T.** 2004. Autophagy: a regulated bulk degradation process inside cells. *Biochem. Biophys. Res. Commun.* **313**: 453–458.
150. **Zhang, X., Z. Zhang, D. Alexander, R. Bracha, D. Mirelman, and S. L. Stanley, Jr.** 2004. Expression of amoebapores is required for full expression of *Entamoeba histolytica* virulence in amebic liver abscess but is not necessary for the induction of inflammation or tissue damage in amebic colitis. *Infect. Immun.* **72**:678–683.
151. **Zhang, J.** 2000. Protein-length distributions for the three domains of life. *Trends Genet.* **16**:107–109.

THE JOURNAL OF BIOLOGICAL CHEMISTRY VOL. 285, NO. 50, pp. 39160–39170, December 10, 2010

Metabolome Analysis Revealed Increase in *S*-Methylcysteine and Phosphatidylisopropanolamine Synthesis upon L-Cysteine Deprivation in the Anaerobic Protozoan Parasite *Entamoeba histolytica*[*] [S]

Received for publication, July 22, 2010, and in revised form, September 23, 2010 Published, JBC Papers in Press, October 5, 2010, DOI 10.1074/jbc.M110.167304

Afzal Husain[‡§1], Dan Sato[¶], Ghulam Jeelani[‡‖2], Fumika Mi-ichi[‡3], Vahab Ali[§4], Makoto Suematsu[‖], Tomoyoshi Soga[¶], and Tomoyoshi Nozaki[‡2,5]

From the [‡]Department of Parasitology, National Institute of Infectious Diseases, 1-23-1 Toyama, Shinjuku-ku, Tokyo 162-8640, Japan, the [§]Department of Parasitology, Gunma University, Graduate School of Medicine, Maebashi 371-8511, Japan, the [¶]Institute for Advanced Biosciences, Keio University, Tsuruoka, Yamagata 997-0052, Japan, and the [‖]Department of Biochemistry and Integrative Medical Biology, School of Medicine, Keio University, Shinjuku, Tokyo 160-8582, Japan

L-Cysteine is ubiquitous in all living organisms and is involved in a variety of functions, including the synthesis of iron-sulfur clusters and glutathione and the regulation of the structure, stability, and catalysis of proteins. In the protozoan parasite *Entamoeba histolytica*, the causative agent of amebiasis, L-cysteine plays an essential role in proliferation, adherence, and defense against oxidative stress; however, the essentiality of this amino acid in the pathways it regulates is not well understood. In the present study, we applied capillary electrophoresis time-of-flight mass spectrometry to quantitate charged metabolites modulated in response to L-cysteine deprivation in *E. histolytica*, which was selected as a model for examining the biological roles of L-cysteine. L-Cysteine deprivation had profound effects on glycolysis, amino acid, and phospholipid metabolism, with sharp decreases in the levels of L-cysteine, L-cystine, and *S*-adenosylmethionine and a dramatic accumulation of *O*-acetylserine and *S*-methylcysteine. We further demonstrated that *S*-methylcysteine is synthesized from methanethiol and *O*-acetylserine by cysteine synthase, which was previously considered to be involved in sulfur-assimilatory L-cysteine biosynthesis. In addition, L-cysteine depletion repressed glycolysis and energy generation, as it reduced acetyl-CoA, ethanol, and the major nucleotide di- and triphosphates, and led to the accumulation of glycolytic intermediates. Interestingly, L-cysteine depletion increased the synthesis of isopropanolamine and phosphatidylisopropanolamine, and it was confirmed that their increment was not a result of oxidative stress but was a specific response to L-cysteine depletion. We also identified a pathway in which isopropanolamine is synthesized from methylglyoxal via aminoacetone. To date, this study represents the first case where L-cysteine deprivation leads to drastic changes in core metabolic pathways, including energy, amino acid, and phospholipid metabolism.

Sulfur-containing amino acids are essential for all living organisms from bacteria to higher eukaryotes and play indispensable roles in various cellular processes, such as methylation and the generation of polyamines, iron-sulfur clusters, and antioxidants. L-Cysteine in particular is essential for the structure, stability, and various protein functions, including catalysis, electron transfer, redox regulation, nitrogen fixation, and sensing for regulatory processes (1).

Entamoeba histolytica is an enteric protozoan parasite that causes hemorrhagic dysentery and extraintestinal abscesses in millions of inhabitants of endemic areas (2). This parasite is generally considered as anaerobic/microaerophilic and has been shown to consume oxygen and tolerate low levels of oxygen pressure but lacks most of the components of antioxidant defense mechanisms, such as catalase, peroxidase, glutathione, and the glutathione-recycling enzymes glutathione peroxidase and glutathione reductase (3, 4). L-Cysteine, which replaces glutathione as a major thiol in *E. histolytica*, is synthesized via a sulfur assimilatory *de novo* cysteine biosynthetic pathway (5–9) that is typically present in bacteria and plants. This pathway consists of two steps that are catalyzed by serine acetyltransferase (SAT, EC 2.3.1.30)[6]

* This work was supported by Grants-in-Aid for Scientific Research 18GS0314, 18050006, and 18073001 (to T. N.) and 20590429 (to D. S.) from the Ministry of Education, Culture, Sports, Science and Technology of Japan, Grant H20-Shinkosaiko-016 for research on emerging and re-emerging infectious diseases from the Ministry of Health, Labour and Welfare of Japan, and a grant for research to promote the development of anti-AIDS pharmaceuticals from the Japan Health Sciences Foundation (to T. N.).

[S] The on-line version of this article (available at http://www.jbc.org) contains supplemental Fig. S1.

[1] Supported by the Monbukagakusho Scholarship from the Ministry of Education, Culture, Sports, Science and Technology.

[2] Supported by the Global Center of Excellence Program for Human Metabolomic System Biology of the Ministry of Education Culture, Sports, Science and Technology.

[3] Present address: Division of Molecular and Cellular Immunoscience, Dept. of Biomolecular Sciences, Saga University, Saga 849-8581, Japan.

[4] Present address: Dept. of Biochemistry, Rajendra Memorial Research Institute of Medical Sciences, Agamkuan, Patna-800007, India.

[5] To whom correspondence should be addressed: Dept. of Parasitology, National Institute of Infectious Diseases, 1-23-1 Toyama, Shinjuku-ku, Tokyo 162-8640, Japan. Tel.: 81-3-5285-1111, Ext. 2600; Fax: 81-3-5285-1219; E-mail: nozaki@nih.go.jp.

[6] The abbreviations used are: SAT, serine acetyltransferase; CS, cysteine synthase; CE-TOFMS, capillary electrophoresis time-of-flight mass spectrometry; 2′,7′-DCF-DA, 2′,7′-dichlorodihydrofluorescein di-acetate; ESI, electrospray ionization; Cho, choline; Cho-P, choline phosphate; OAS, *O*-acetylserine; SMC, *S*-methylcysteine; SAM, *S*-adenosylmethionine; Ispn, isopropanolamine; Ispn-P, isopropanolamine phosphate; PtdIspn, phosphatidylisopropanolamine; Etn, ethanolamine; Etn-P, ethanolamine phosphate; PtdEtn, phosphatidylethanolamine.

(7, 8) and cysteine synthase (CS; OAS (thiol) lyase; EC 4.2.99.8) (5). In addition to the presence of prokaryotic/plant-like L-cysteine biosynthesis, *E. histolytica* is also unique because the forward and reverse trans-sulfuration pathways are absent and interrupted, respectively. Furthermore, through lateral gene transfer from archaea, *E. histolytica* has acquired methionine γ-lyase (EC 4.4.1.11), an enzyme that degrades L-methionine, L-homocysteine, and L-cysteine (10–12). Thus, although typical parasitic protists show degenerated amino acid metabolic pathways, particularly those associated with catabolism, because of the parasitic lifestyle, sulfur-containing amino acid metabolism appears to have uniquely evolved in *E. histolytica*. However, the specific role of this pathway in this organism remains unclear.

L-Cysteine is the principal low molecular weight thiol in *E. histolytica* and is involved in the survival, growth, attachment, elongation, motility, gene regulation, and antioxidative stress defense of this organism (13–17). Because sulfur-containing amino acid metabolism differs significantly between *E. histolytica* and its mammalian host, the molecular dissection and characterization of this pathway may lead to the development of new chemotherapeutics against this parasite (18).

Here, to gain further insight into the roles and regulatory mechanisms of sulfur-containing amino acid metabolism and individual metabolites in *E. histolytica*, we utilized capillary electrophoresis time-of-flight mass spectrometry (CE-TOFMS) (19–21) for the metabolomic profiling of this parasite. We observed drastic changes in the metabolome as a result of L-cysteine depletion, which led to the discovery of novel L-cysteine-mediated regulation of several metabolic pathways in *E. histolytica*.

EXPERIMENTAL PROCEDURES

Chemicals and Reagents—All of the chemicals of analytical grade were purchased from either Wako or Sigma-Aldrich unless otherwise mentioned. 2′,7′-Dichlorodihydrofluorescein di-acetate (2′,7′-DCF-DA) was purchased from Invitrogen. 1-Aminoacetone hydrochloride was obtained from United States Biologicals. High performance thin layer chromatography silica gel 60 plates were purchased from Merck. [U-$^{13}C_5$,^{15}N]L-Methionine and [U-$^{13}C_3$,^{15}N]L-serine were purchased from Cambridge Isotope Laboratories. Stock solutions of metabolite standards (1–100 mmol/liter) for CE-MS analysis were prepared in either Milli-Q water, 0.1 mol/liter HCl, or 0.1 mol/liter NaOH. A mixed solution of the standards was prepared by diluting stock solutions with Milli-Q water immediately before CE-TOFMS analysis.

Microorganisms and Cultivation—Trophozoites of the *E. histolytica* clonal strain HM-1: IMSS cl 6 were maintained axenically in Diamond's BI-S-33 medium at 35.5 °C, as described previously (22, 23). Trophozoites were harvested in the late logarithmic growth phase 2–3 days after the inoculation of medium with one-thirtieth to one-twelfth of the total culture volume.

Metabolic Labeling and Metabolite Extraction—*E. histolytica* trophozoites were cultivated in either standard BI-S-33 medium containing 8 mM L-cysteine or L-cysteine-deprived medium for 48 h. For the metabolic labeling, trophozoites were cultured in the presence of either 3 mM stable isotope-labeled [U-$^{13}C_5$,^{15}N]L-methionine or 6 mM [U-$^{13}C_3$,^{15}N]L-serine in L-cysteine-deprived medium for 48 h as described above. To extract metabolites, ~1.5×10^6 cells from each condition were harvested and washed twice with 5% mannitol. The cells were then suspended in 1.6 ml of methanol containing 16 μM of each internal standard, 2-(*N*-morpholino)ethanesulfonic acid, methionine sulfone, and D-camphor-10-sulfonic acid and mixed with 1.6 ml of chloroform and 640 μl of deionized water. After vortexing, the mixture was centrifuged at 4,600 × *g* at 4 °C for 5 min. The aqueous layer (1.6 ml) was filtrated using an Amicon Ultrafree-MC ultrafilter (Millipore Co.) and centrifuged at 9,100 × *g* at 4 °C for ~2 h. The filtrate was dried and preserved at −80 °C until mass spectrometric analysis (24). Prior to the analysis, the sample was dissolved in 20 μl of deionized water containing reference compounds (200 μmol/liter each of 3-aminopyrrolidine and trimesic acid).

Instrumentation and CE-TOFMS Conditions—CE-TOFMS was performed using an Agilent CE capillary electrophoresis system equipped with an Agilent 6210 time-of-flight mass spectrometer, Agilent 1100 isocratic HPLC pump, Agilent G1603A CE-MS adapter kit, and Agilent G1607A CE-ESI-MS sprayer kit (Agilent Technologies, Waldbronn, Germany). The system was controlled by Agilent G2201AA ChemStation software for CE. Data acquisition was performed by Analyst QS software for Agilent TOF (Applied Biosystems and MDS Sciex).

CE-TOFMS Conditions for Cationic Metabolite Analysis—Cationic metabolites were separated in a fused silica capillary (50-μm inner diameter × 100-cm) filled with 1 mol/liter formic acid as the reference electrolyte (25). Sample solution (~3 nl) was injected at 50 mbar for 3 s, and a positive voltage of 30 kV was applied. The capillary and sample trays were maintained at 20 °C and below 5 °C, respectively. Sheath liquid composed of methanol/water (50% v/v) that contained 0.1 μmol/liter hexakis (2,2-difluorothoxy)phosphazene was delivered at 10 μl/min. ESI-TOFMS was operated in the positive ion mode. The capillary voltage was set at 4 kV, and a flow rate of nitrogen gas (heater temperature, 300 °C) was set at 10 p.s.i. For TOFMS, the fragmenter voltage, skimmer voltage, and octapole radio frequency voltage (Oct RFV) were set at 75, 50, and 125 V, respectively. An automatic recalibration function was performed using two reference masses of reference standards; protonated [^{13}C]methanol dimer (*m/z* 66.063061) and protonated hexakis (2,2-difluorothoxy)phosphazene (*m/z* 622.028963), which provided the lock mass for exact mass measurements. Exact mass data were acquired at the rate of 1.5 cycles/s over a 50–1,000 *m/z* range.

CE-TOFMS Conditions for Anionic Metabolite Analysis—Anionic metabolites were separated in a cationic polymer-coated COSMO(+) capillary (50-μm inner diameter × 110-cm) (Nacalai Tesque) filled with 50 mmol/liter ammonium acetate solution, pH 8.5, as the reference electrolyte (26, 27). Sample solution (~30 nl) was injected at 50 mbar for 30 s, and a negative voltage of −30 kV was applied. Ammonium acetate (5 mmol/liter) in methanol/water (50% v/v) that contained 0.1 μmol/liter hexakis (2,2-difluorothoxy)phosphazene was delivered as sheath liquid at 10 μl/min. ESI-TOFMS was operated

in the negative ion mode. The capillary voltage was set at 3.5 kV. For TOFMS, the fragmenter voltage, skimmer voltage, and Oct RFV were set at 100, 50, and 200 V, respectively (27). An automatic recalibration function was performed using two reference masses of reference standards: deprotonated ^{13}C acetate dimer (*m/z* 120.038339) and acetate adduct of hexakis (2,2-difluorothoxy)phosphazene (*m/z* 680.035541). The other conditions were identical to those used for the cationic metabolite analysis.

CE-TOFMS Data Processing—Raw data were processed using the in-house software Masterhands (28). The overall data processing flow consisted of the following steps: noise filtering, baseline removal, migration time correction, peak detection, and integration of peak area from a 0.02 *m/z*-wide slice of the electropherograms. This process resembled the strategies employed in widely used data processing software for LC-MS and GC-MS data analysis, such as MassHunter (Agilent Technologies) and XCMS (29). Subsequently, accurate *m/z* values for each peak were calculated by Gaussian curve fitting in the *m/z* domain, and migration times were normalized using alignment algorithms based on dynamic programming (19, 30). All of the target metabolites were identified by matching their *m/z* values and normalized migration times with those of standard compounds in the in-house library.

Quantitation of Reactive Oxygen Species—Fluorescence spectrophotometry was used to measure the production of intracellular reactive oxygen species using 2′,7′-DCF-DA as a probe as previously described (31). Briefly, *E. histolytica* cells were washed in PBS, and 5.0×10^5 cells were then incubated in 1 ml of PBS containing 20 μM 2′,7′-DCF-DA for 30 min at 35.5 °C in the dark. The intensity of fluorescence was immediately read at excitation and emission wavelengths of 492 and 519 nm, respectively.

L-Cysteine/SMC Synthase Assay—L-Cysteine/SMC synthase was assayed by measuring acetate production through the coupling reaction of this enzyme with acetate kinase, pyruvate kinase, and lactate dehydrogenase. Acetate kinase generates ADP and acetyl-phosphate from acetate and ATP. The ADP production was coupled with the oxidation of NADH (ϵ_{340} = 6.22 mM^{-1} cm^{-1}) through pyruvate kinase and lactate dehydrogenase (32). The standard reaction mixture contained 50 mM of Tris-Cl, pH 8.0, 3 mM OAS, 3 mM sodium sulfide or sodium methanethiolate, 4 units each of acetate kinase, pyruvate kinase, and lactate dehydrogenase, 0.5 mM ATP, 0.3 mM NADH, and 1–2 μg of recombinant cysteine synthase. The reactions were initiated by the addition of recombinant cysteine synthase, and optical absorbance was read at 340 nm on a Shimadzu spectrophotometer. Kinetic parameters were determined using various concentrations (0.1–6 mM) of sodium sulfide, sodium methanethiolate, and OAS. The kinetic parameters were estimated using the nonlinear regression function obtained from the GraphPad Prism software (GraphPad Software Inc., San Diego, CA).

Choline and Ethanol Quantitation—The amount of choline (Cho) in the metabolite extracts was quantitated enzymatically using components of the Amplex® Red sphingomyelinase assay kit (Invitrogen). Briefly, Cho was first oxidized by Cho oxidase to betaine and hydrogen peroxide. The produced hydrogen peroxide was then reacted with Amplex® Red reagent in a 1:1 stoichiometry in the presence of horseradish peroxidase to generate the highly fluorescent product resorufin, which was read in a fluorescence spectrophotometer (model F-2500; Hitachi) at excitation and emission wavelengths of 545 and 590 nm, respectively. Ethanol production by trophozoites cultured in either normal or L-cysteine-deprived medium was determined as described previously (33).

Extraction of Lipids, Thin Layer Chromatography, and Phospholipid Quantitation—Cells cultured in either normal or cysteine-deprived medium for 48 h were collected by centrifugation, and lipids were then extracted by the Bligh and Dyer's method (34). The extracted lipids were analyzed by two-dimensional high performance thin layer chromatography using a solvent system of chloroform:methanol:28% ammonium hydroxide (65:25:5 v/v/v) in the first direction and chloroform:acetone:methanol:Acetic acid:water (50:20:10:10:5 v/v/v/v/v) in the second. The phosphorus content of phospholipids was determined after scraping representative spots from the plate, as described previously (35). The lipids were visualized by exposing TLC plates to iodine vapor.

RESULTS

L-Cysteine Deprivation Caused Accumulation of O-Acetylserine and S-Methylcysteine—We first verified that L-cysteine deprivation affected intracellular L-cysteine/L-cystine concentrations in *E. histolytica*. Under normal culture conditions (8 mM L-cysteine), the intracellular concentrations of L-cysteine and L-cystine were 431 ± 52 and 202 ± 40 pmol, respectively, per 2×10^5 cells. Approximately two-thirds (68 ± 7%) of L-cysteine/L-cystine was present in a reduced form, whereas the remaining third was present in an oxidized form. Upon L-cysteine deprivation for 48 h, both L-cysteine and L-cystine decreased to nearly undetectable levels (88 ± 11 and 79 ± 10% decrement, respectively) (Fig. 1*A*). These results suggest that the intracellular L-cysteine/L-cystine concentrations in *E. histolytica* are greatly affected by the composition of the extracellular milieu.

We also examined whether oxidative stress induced by paraquat affected intracellular L-cysteine/L-cystine concentrations. Treatment of the amebae with 2 mM paraquat for 10 h led to 60.6 ± 8.8 and 41.4 ± 7.3% decreases in the levels of L-cysteine and L-cystine, respectively. Under conditions of L-cysteine limitation, the intracellular levels of reactive oxygen species increased by >4-fold, which was comparable with the 3.3-fold increase observed in paraquat/air-treated cells (Fig. 1*B*). These results suggest that L-cysteine may be an important scavenger of reactive oxygen species in *E. histolytica*.

Among the ~90 intermediary metabolites that were measured by CE-TOFMS-based metabolomic analysis, which include amino acids, organic acids, and nucleotides (19–21), L-cysteine depletion caused drastic changes in the metabolites of *E. histolytica* involved in sulfur-containing amino acid metabolism (Fig. 1*C*). L-Cysteine depletion resulted in a sharp increase in *O*-acetylserine (OAS) (nearly undetectable under normal conditions), an activated form of L-serine that is synthesized from L-serine and acetyl-CoA by SAT. We also ob-

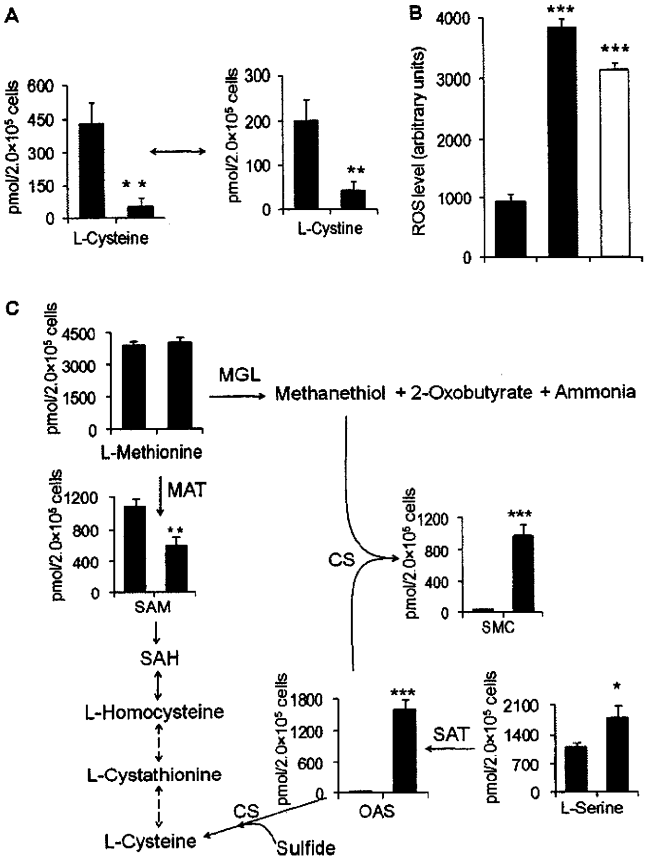

FIGURE 1. **Effects of L-cysteine depletion on the content of L-cysteine/L-cystine, reactive oxygen species, and metabolites in sulfur-containing amino acid metabolism in *E. histolytica*.** Trophozoites were cultured in normal (*black bars*) or cysteine-deprived medium (*gray bars*) for 48 h, or normal medium containing 2 mM paraquat (*white bars*) for 10 h. *Asterisks* (*, **, and ***) denote statistically significant differences with $p \leq 0.05$, $p \leq 0.01$, and $p \leq 0.001$, respectively, as determined by Student's *t* test, and all of the experiments were performed in triplicate. *A*, effects of L-cysteine depletion on intracellular L-cysteine and L-cystine concentrations. The average content (pmol) ± S.D (*error bars*) in 2×10^5 cells is shown. *B*, effects of L-cysteine depletion (72 h) and oxidative stress on the level of reactive oxygen species. The average level of 2′,7′-DCF-DA fluorescence (arbitrary units) ± S.D. (*error bars*) of 5×10^5 cells is shown. *C*, effects of L-cysteine depletion on the level of metabolites involved in sulfur-containing amino acid metabolism. The average content (pmol) ± S.D. (*error bars*) in 2×10^5 cells, performed in triplicate, is shown. *SAH*, *S*-adenosylhomocysteine; *MAT*, L-methionine adenosyltransferase; *MGL*, L-methionine γ-lyase.

served a marked increase (nearly undetectable under normal conditions) in *S*-methylcysteine (SMC), which is suggested to be a storage compound for sulfide and methyl groups in plants (36). L-Cysteine deprivation also caused a 44 ± 6% decrement in the level of *S*-adenosylmethionine (SAM), whereas the level of L-methionine remained unchanged.

SMC can be formed by the methylation of L-cysteine using either SAM or *S*-methylmethionine as a methyl group donor or by the transfer of the alanyl moiety of OAS to methanethiol (CH_3SH) by CS (37). To differentiate between these possibilities, we performed metabolic labeling of *E. histolytica* trophozoites with stable isotope U-^{13}C,^{15}N-labeled L-serine and L-methionine in normal and L-cysteine-depleted media for 48 h. Upon the addition of [U-$^{13}C_3$,^{15}N]Ser to the L-cysteine-depleted culture medium, comparable levels of [$^{13}C_3$,^{15}N]SMC and unlabeled SMC, derived from [U-$^{13}C_3$,^{15}N]OAS and unlabeled OAS, respectively, were detected (Fig. 2*A*). Similarly, when trophozoites were cultured in the presence of [U-$^{13}C_5$,^{15}N]Met under the L-cysteine-deprived conditions, we also detected comparable levels of [$^{13}C_1$]SMC and unlabeled SMC (Fig. 2*B*). In contrast, under normal conditions, neither SMC nor OAS was detected after [U-$^{13}C_3$,^{15}N]Ser or [U-$^{13}C_5$,^{15}N]Met labeling (data not shown). Taken together, these data clearly indicate that SMC is not synthesized by SAM- or *S*-methylmethionine-dependent methylation of L-cysteine; rather, SMC is synthesized in *E. histolytica* from the backbone of Ser and thiomethyl group of methanethiol.

Surprisingly, [$^{13}C_3$,^{15}N]OAS was not incorporated into either L-cysteine or L-cystine (data not shown), or their levels were too low to be detected by CE-TOFMS. To determine whether the lack of OAS incorporation into L-cysteine was due to the low sulfide concentrations under the *in vitro* axenic growth conditions, we deprived trophozoites of L-cysteine for 45 h and then continued their culture in medium supplemented with 2 mM sulfide for a further 3 h. However, sulfide supplementation did not affect the level of L-cysteine, whereas the levels of SMC and OAS markedly decreased (90.6 ± 3.4 and 84.8 ± 7.7% decrement, respectively) compared with the unsupplemented medium (Fig. 2*C*). These data suggest that sulfide negatively regulates OAS and SMC synthesis and also imply that the pathway formally called the "L-cysteine biosynthetic pathway" is primarily involved in the synthesis of SMC, but not L-cysteine, at least under *in vitro* culture conditions.

In Vitro Examination of S-Methylcysteine Synthesis—To elucidate the enzyme(s) involved in the formation of SMC from OAS and methanethiol, we examined whether different CS isotypes could catalyze the synthesis of SMC. Among the three examined CS isotypes (EhCS1–3), two CS proteins (EhCS1 and EhCS2) are very similar (99% amino acid identity, with two conserved amino acid changes) (5, 6), whereas EhCS3 shares only 83% amino acid identity with the other two isotypes. Both recombinant EhCS1 and EhCS3 efficiently catalyzed the synthesis of SMC using OAS and methanethiol as substrates. As revealed from the kinetic parameters (Fig. 2*D*), EhCS1 and EhCS3 did not show any preference for either methanethiol or sulfide, because the K_m, V_{max}, k_{cat}, and k_{cat}/K_m values for both of these substrates were comparable.

L-Cysteine Depletion Repressed Glycolysis and Energy Generation—Similar to other anaerobic and microaerophilic parasitic protozoa, such as *Giardia lamblia* and *Trichomonas vaginalis*, *E. histolytica* lacks features of aerobic eukaryotic metabolism, including the TCA cycle and oxidative phosphorylation, and primarily generates energy by substrate level phosphorylation (10). The CE-TOFMS-based metabolomic analysis demonstrated that L-cysteine depletion affected the levels of the majority of metabolites involved in glycolysis and its associated pathways (Fig. 3). L-Cysteine-depleted amebae generally contained higher amounts of glycolytic intermediates, with the exception of acetyl CoA and ethanol, than cells cultured under normal conditions. The largest changes caused by L-cysteine depletion were the increment in the levels of glycerol-3-phosphate (2.18 ± 0.25-fold), *O*-phosphoserine (1.70 ± 0.22-fold), pyruvate (1.66 ± 0.26-fold), 3-phosphoglycerate (1.60 ± 0.17-fold), malate (1.50 ± 0.20-fold),

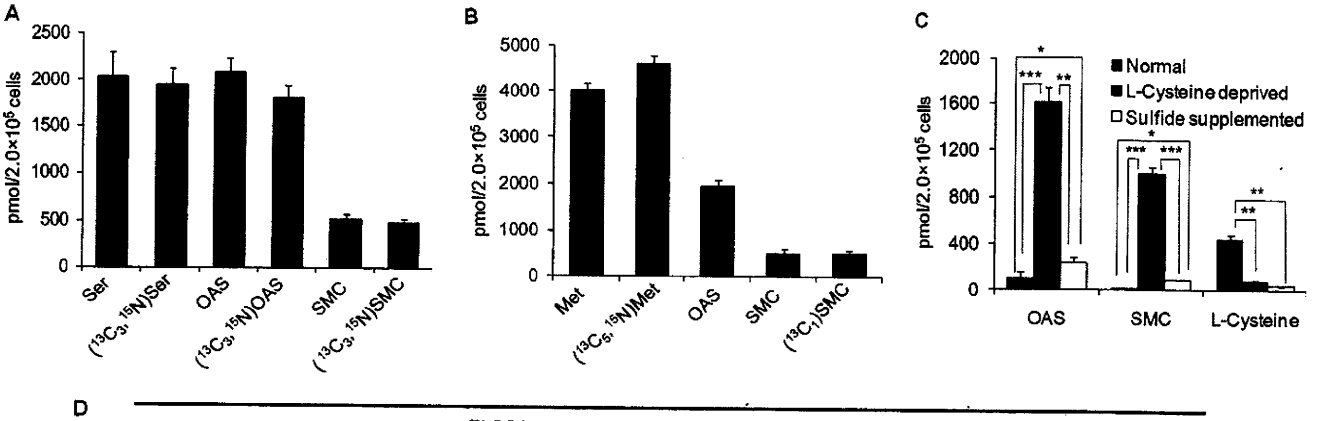

D

	EhCS1				EhCS3			
	Km (mM)	*Vmax* (μmol/min/mg)	*kcat* (s^{-1})	*Kcat/Km* ($mM^{-1}s^{-1}$)	*Km* (mM)	*Vmax* (μmol/min/mg)	*kcat* (s^{-1})	*Kcat/Km* ($mM^{-1}s^{-1}$)
OAS	2.34±0.32	36.20±5.43	22.07±3.26	9.43±2.12	2.54±0.28	31.96±.4.68	19.37±2.98	7.61±2.09
Sulfide	2.01±0.40	35.59±6.21	21.71±3.98	10.81±2.33	2.23±0.34	31.42±5.79	19.08±3.56	8.56±2.24
Methanethiolate	1.66±0.39	25.51±4.78	15.57±2.84	9.37±3.08	2.11±0.39	21.74±3.94	11.22±2.37	5.32±1.88

FIGURE 2. **Examination of *S*-methylcysteine biosynthesis in *E. histolytica*.** *A* and *B*, incorporation of labeled L-serine and L-methionine into *S*-methylcysteine. Trophozoites were cultured in the presence of 6 mM [U-$^{13}C_3$, ^{15}N]L-serine (*A*) or 3 mM [U-$^{13}C_5$, ^{15}N]L-methionine (*B*) in L-cysteine-deprived medium for 48 h. The average contents (pmol) ± S.D. (*error bars*) of unlabeled and labeled amino acids and their derivatives in 2 × 10^5 trophozoites, performed in triplicate, are shown. *C*, effects of the supplementation of the medium with sodium sulfide (2 mM) on the levels of OAS, SMC, and L-cysteine, under conditions of L-cysteine deprivation. *Asterisks* (*, **, and ***) denote statistically significant differences with $p \leq 0.05$, $p \leq 0.01$, and $p \leq 0.001$, respectively, as determined by Student's *t* test. *D*, kinetic parameters of recombinant cysteine synthase 1 (EhCS1) and 3 (EhCS3). All of the reactions were performed in triplicate as described under "Experimental Procedures," and the values are expressed as the means ± S.D.

and fumarate (1.60 ± 0.20-fold). Several other metabolites involved in glycolysis, including glucose 6-phosphate, glucose 1-phosphate, fructose 6-phosphate, and phosphoenolpyruvate also showed slightly elevated levels (1.2–1.5-fold), whereas the levels of fructose 1,6-bisphosphate and dihydroxyacetone-phosphate remained unchanged. In contrast to the significant increases in the glycolytic intermediates upstream of pyruvate in amebae cultured under L-cysteine-limited conditions, we observed reduced levels of acetyl CoA (29.4 ± 7.1%) and ethanol (40.7 ± 6.7%), suggesting a decrease in glycolytic flux and ATP generation by L-cysteine depletion. A number of other metabolites downstream of acetyl CoA, such as *N*-acetyl-glutamate, *N*-acetyl β-alanine, *N*-acetyl-leucine, and *N*-acetyl-phenylalanine, were also decreased (supplemental Fig. S1), supporting the premise that the glycolytic flux downstream of pyruvate was repressed.

Because glycolysis is the major source of energy generation in *E. histolytica*, a reduced glycolytic flux was thought to result in a decrement in the energy storage molecules of the trophozoites. As expected, the levels of the nucleotide triphosphates ATP, GTP, UTP, and CTP were significantly lower ($p \leq 0.05$) in the L-cysteine-depleted cells than in the trophozoites maintained under normal conditions (Fig. 3). We also observed slight deceases in the levels of ADP and GDP, whereas the levels of AMP and GMP were unchanged (Fig. 3).

L-Cysteine Depletion Altered Amino Acid Pools—Because amino acids are also used for energy production in *E. histolytica* (38), we examined the effects of L-cysteine deprivation on amino acid levels (supplemental Fig. S1). Next to L-cysteine and L-cystine, L-threonine and L-serine were the most highly modulated by L-cysteine depletion (1.63 ± 0.25- and 2.07 ± 0.29-fold increases, respectively) among the 20 amino acids. In *E. histolytica*, L-threonine and L-serine are catabolized by threonine dehydratase (39) to yield 2-oxobutyrate and pyruvate, respectively, which are in turn used by pyruvate:ferredoxin oxidoreductase for energy generation (40). L-Cysteine depletion also resulted in a slight increase in the intracellular concentration of L-alanine, which is synthesized from pyruvate by L-alanine:2-oxoglutarate aminotransferase (EHI_096750 (EAL50292.1) and EHI_159710 (EAL44861.1)). The levels of the remaining amino acids were not significantly affected by L-cysteine depletion.

L-Cysteine Depletion Caused Increases in Isopropanolamine, Aminoalcohol Phosphates, and Phosphatidylisopropanolamine—The metabolomic analysis of *E. histolytica* also revealed that L-cysteine depletion caused marked changes in amino alcohol metabolism (Fig. 4*A*). L-Cysteine depletion led to a dramatic increase in the levels of isopropanolamine (1-aminopropan-2-ol, Ispn) (5.44 ± 0.76-fold) and isopropanolamine phosphate (Ispn-P, undetected under normal conditions) (Fig. 4*A*). In addition, trophozoites cultured in L-cysteine-limited conditions showed 7.01 ± 1.38- and 2.8 ± 0.21-fold increases in ethanolamine phosphate (Etn-P) and choline phosphate (Cho-P) levels, respectively, whereas the levels of ethanolamine (Etn) and Cho were unchanged. Both Etn-P and Cho-P are intermediates in the Kennedy pathway,

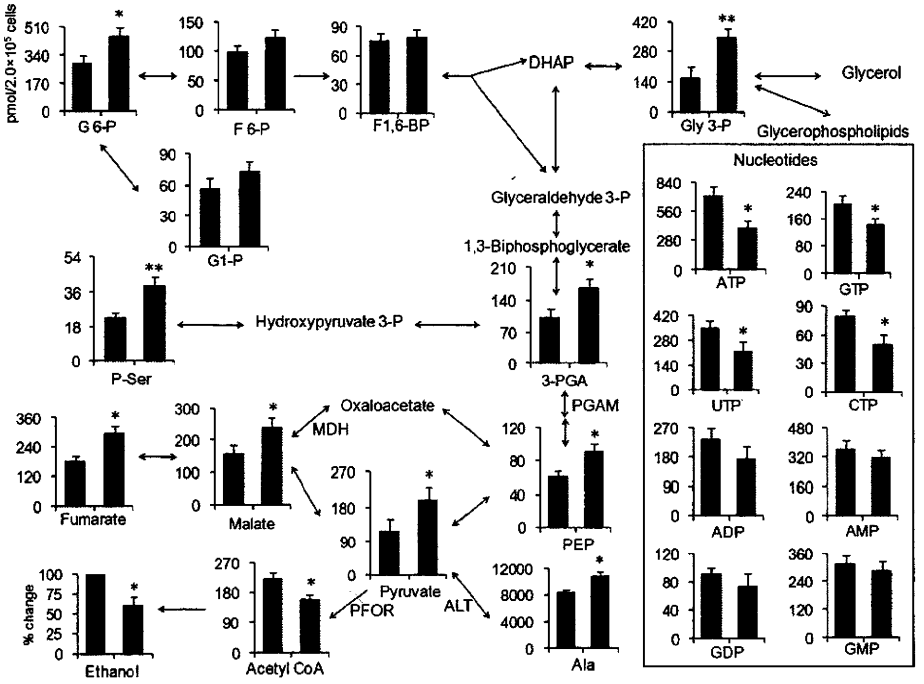

FIGURE 3. **Effects of L-cysteine depletion on the level of metabolites involved in central energy metabolism.** Trophozoites were cultured in normal (*black bars*) or cysteine-deprived medium for 48 h (*gray bars*), and the average contents (pmol) ± S.D. (*error bars*) of the indicated metabolites in 2×10^5 cells are shown (performed in triplicate). Nucleotide metabolites are *boxed*. Ethanol is shown as a percentage change. *Asterisks* (* and **) denote statistically significant differences with $p \leq 0.05$ and $p \leq 0.01$, respectively, as determined by Student's *t* test. *PFOR*, pyruvate:ferredoxin oxidoreductase; *ALT*, L-alanine: 2-oxoglutarate aminotransferase; *PGAM*, phosphoglycerate mutase; *MDH*, malate dehydrogenase; *G 6-P*, glucose 6-phosphate; *G1-P*, glucose 1-phosphate; *F 6-P*, fructose 6-phosphate; *F1,6-BP*, fructose 1,6-biphosphate; *Gly 3-P*, glycerol 3-phosphate; *3-PGA*, 3-phosphoglycerate; *PEP*, phosphoenolpyruvate; *P-Ser*, *O*-phosphoserine.

where phospholipids, including phosphatidylethanolamine and phosphatidylcholine, are produced.

Because L-cysteine limitation affected Ispn-P, Etn-P, and Cho-P concentrations, we next investigated whether L-cysteine deprivation influenced phospholipid synthesis by performing lipid profiling of amebic trophozoites cultured under L-cysteine-deprived or normal conditions using two-dimensional TLC (Fig. 4*B*). We found that in the absence of L-cysteine, *E. histolytica* synthesized an unconventional phospholipid that was verified to be phosphatidylisopropanolamine (PtdIspn) and was undetectable under normal conditions. Quantitation of individual lipids indicated that phosphatidylethanolamine (PtdEtn) decreased by 39.9 ± 6.9%, whereas other phospholipids, such as phosphatidylcholine (PtdCho), phosphatidylserine, phosphatidylinositol, and phosphatidic acid, were unchanged (Fig. 4*C*). These data are consistent with the premise that PtdIspn was formed in a competition for the formation of PtdEtn, the level of which decreased by approximately the identical amount that PtdIspn increased (Fig. 4*C*). To further demonstrate that PtdIspn was formed from Ispn, *E. histolytica* trophozoites were cultured in normal medium containing 5 mM Ispn for 24 h. Under this condition, trophozoites produced an appreciable amount of PtdIspn (Fig. 4*B*, *panel c*).

As described above, L-cysteine depletion increased the level of reactive oxygen species. We therefore examined whether oxidative stress caused the observed changes in amino alcohols and phospholipids. It was observed that the lipid profiling of *E. histolytica* trophozoites cultured with 2 mM paraquat in ambient air for 10 h did not increase PtdIspn (Fig. 4*B*, *panel e*). Furthermore, the addition of D-cysteine to the L-cysteine-lacking medium did not reverse the effects of L-cysteine deprivation on the phospholipid profiles (Fig. 4*B*, *panel d*). These results confirmed that the generation of PtdIspn caused by L-cysteine depletion was not a result of oxidative stress but represents a specific response to L-cysteine deprivation.

Examination of Isopropanolamine Biosynthesis in E. histolytica—Next, we investigated the synthesis route of Ispn in *E. histolytica*. From studies of *Escherichia coli*, it is known that Ispn is synthesized from 1-aminoacetone by the action of Ispn:NAD^+ oxidoreductase (41). 1-Aminoacetone is formed by the breakdown of L-threonine by L-threonine dehydrogenase (42) or is alternatively synthesized from methylglyoxal by monoamine oxidase, which catalyzes the interconversion of methylglyoxal and aminoacetone (43). Methylglyoxal is a by-product of several metabolic pathways, with glycolysis being the most important source (44). Methylglyoxal is synthesized either enzymatically or nonenzymatically from dihydroxyacetone phosphate or glyceraldehyde 3-phosphate (44).

To examine the Ispn synthesis pathway in *E. histolytica*, we cultured amebae in medium supplemented with either methylglyoxal, aminoacetone, or L-threonine and examined the resulting lipid profiles. We found that supplementation with 2 mM methylglyoxal or 4 mM aminoacetone, but not 50 mM L-threonine, led to the synthesis of PtdIspn (Fig. 5*A*). These results are consistent with the premise that *E. histolytica* is capable of Ispn synthesis from methylglyoxal and possesses the

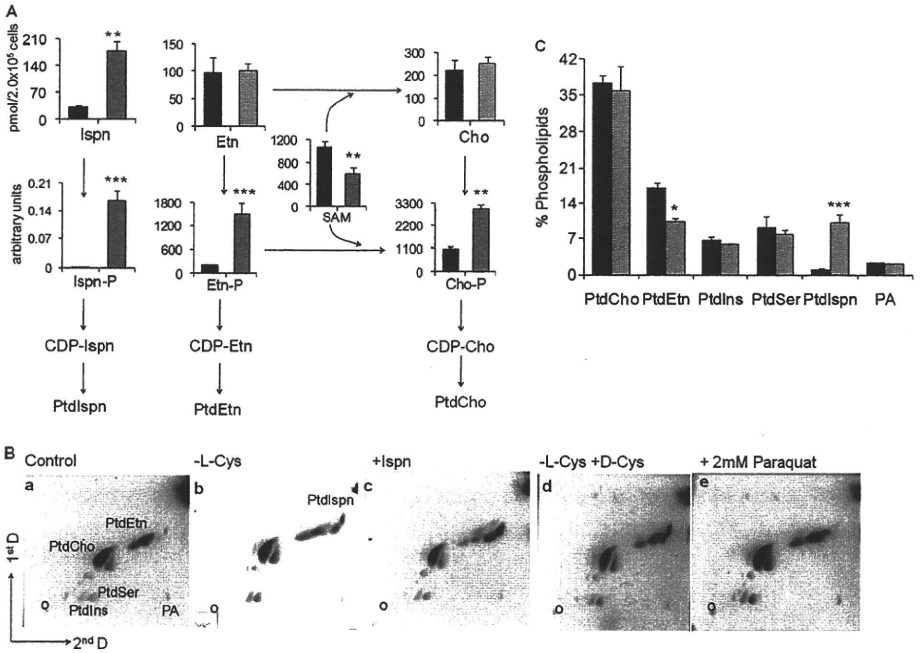

FIGURE 4. **L-Cysteine depletion affected phospholipid metabolism.** *A*, effects of L-cysteine depletion on the levels of metabolites involved in the Kennedy pathway of phospholipid metabolism. Trophozoites were cultured in normal (*black bars*) or cysteine-deprived medium for 48 h (*gray bars*). The average contents (pmol) ± S.D. (*error bars*) in 2×10^5 cells in triplicate are shown. *Asterisks* (*, **, and ***) denote statistically significant differences with $p \leq 0.05$, $p \leq 0.01$, and $p \leq 0.001$, respectively, as determined by Student's *t* test. *B*, profiles of phospholipids derived from trophozoites cultured under various conditions (*panels a–e*), analyzed by two-dimensional TLC. Trophozoites were cultured in normal culture medium (*panels a*, *c*, and *e*) or L-cysteine-deprived medium supplemented (*panels b* and *d*), without (*panels a* and *b*) or with 5 mM Ispn (*panels c*), or 8 mM D-cysteine (*panels d*) for 48 h or 2 mM paraquat for 10 h (*panels e*). *Circles* in the *bottom left corners* indicate the spots where the samples were applied. *C*, quantitation of the phospholipid species (percentage) derived from trophozoites cultured using normal (*black bars*) or L-cysteine-depleted (*gray bars*) medium. *Asterisks* (* and ***) denote statistically significant differences with $p \leq 0.05$ and $p \leq 0.001$, respectively, as determined by Student's *t* test. *PtdSer*, phosphatidylserine; *PtdIns*, phosphatidylinositol; *PA*, phosphatidic acid.

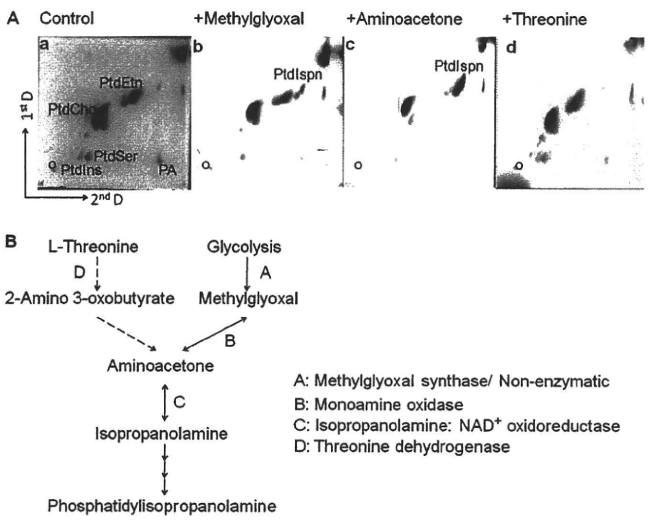

FIGURE 5. **Examination of isopropanolamine biosynthesis in *E. histolytica*.** *A*, effects of the supplementation of potential precursors to the culture medium on the synthesis of phosphatidylisopropanolamine. Trophozoites were cultured in normal culture medium supplemented without (*panel a*) or with 2 mM methylglyoxal (*panel b*), 5 mM aminoacetone (*panel c*), or 50 mM L-threonine for 24 h (*panel d*), and the lipids were then analyzed by two-dimensional TLC. *Circles* in the *bottom left corners* indicate the spots where the samples were applied. *B*, possible pathways of isopropanolamine biosynthesis. The reactions depicted by *solid arrows* were demonstrated in this study, whereas those indicated by *broken arrows* are considered to be absent in *E. histolytica*. *PtdSer*, phosphatidylserine; *PtdIns*, phosphatidylinositol; *PA*, phosphatidic acid.

enzymatic activities of monoamine oxidase and Ispn:NAD^+ oxidoreductase (Fig. 5*B*).

DISCUSSION

Identification of SMC and OAS as the Major Metabolites Increased upon L-Cysteine Deprivation—In the present study, using a CE-TOFMS-based approach (19–21), we identified novel metabolic changes caused by L-cysteine deprivation in the anaerobic/microaerophilic protozoan parasite *E. histolytica*. The major advantages of CE-MS analysis include its extremely high resolution and ability to simultaneously quantify charged low molecular weight compounds (19–21). We demonstrated that L-cysteine deprivation causes a dramatic accumulation of SMC and OAS (Fig. 1*C*). SMC is a sulfur-containing amino acid that has never been detected in protozoa but is widely present in relatively large amounts in several legumes, where it is considered to serve as a sulfur storage compound (36, 37). Using stable isotope-labeled L-serine and L-methionine, we showed that SMC is synthesized from these amino acids in *E. histolytica* via OAS and methanethiol, respectively, which is similar to the pathway reported in *A. thaliana* (36). Interestingly, the increase in both SMC and OAS was mitigated by supplementation of the culture medium with 2 mM sulfide. These results have solved one enigma concerning the biological roles of the sulfur assimilatory *de novo* L-cysteine biosynthetic pathway in *E. histolytica*.

Role of L-Cysteine Biosynthetic Pathway—Although *E. histolytica* is a unique organism that constitutively expresses high

levels of multiple cytosolic isotypes of CS and SAT, the physiological significance of the L-cysteine pathway and its redundancy are not well understood (8, 9, 18). *In vitro* cultivation of amebic trophozoites requires high concentrations of L-cysteine, which cannot be replaced by other thiols (16), indicating that the synthesis pathway may not be sufficient for the production of L-cysteine and might play an unknown role. Our metabolomic study using labeled L-serine did not support the hypothesis that L-cysteine is formed from L-serine and sulfide via OAS by the sequential action of SAT and CS, because labeled L-serine was not incorporated into L-cysteine (data not shown). We also demonstrated that amebic CS isotypes can catalyze the formation of SMC from OAS and methanethiol, unlike the CS from *T. vaginalis* (45), and also possess robust L-cysteine forming activity (Fig. 2*D*).

We also revealed that OAS is exclusively directed for the synthesis of SMC, but not L-cysteine, even in the presence of high concentrations of substrates. The apparent inability of *E. histolytica* to incorporate OAS into L-cysteine under L-cysteine-deprived conditions cannot be explained by the limiting concentration of sulfide under axenic culture conditions because the addition of sulfide did not increase L-cysteine levels, whereas the accumulation of OAS and SMC was immediately ceased by sulfide supplementation (Fig. 2*C*). In fact, the amebic trophozoites cultured under normal conditions contained appreciable concentrations of sulfide (134 μM) (46). The lack of OAS incorporation into L-cysteine is also not attributable to the low substrate specificity of CS toward sulfide, because the K_m values of CS isotypes for sulfide were comparable with those for methanethiolate (Fig. 2*D*). Thus, the preferred utilization of OAS by *E. histolytica* for SMC synthesis, but not for L-cysteine production, suggests that the L-cysteine biosynthetic pathway plays a major role in SMC production, whereas the apparent defect of L-cysteine production by this pathway *in vivo* remains puzzling.

Regulation of OAS Synthesis—The marked increase in OAS observed under L-cysteine deprivation is also worthy of attention. Similar to SMC, the level of OAS under normal culture conditions was nearly undetectable. Unlike other organisms, *E. histolytica* possesses three apparently functionally redundant, cytosolic SAT isozymes (SAT1–3) (9). Because these SAT isozymes have low to high sensitivity to feedback inhibition by L-cysteine, OAS and SMC were presumed to be formed even in the presence of high concentrations of L-cysteine, mainly by L-cysteine-insensitive SAT3. Thus, the fact that OAS and SMC were undetectable in the amebae cultured under normal conditions indicates that the activity of SAT, particularly SAT3, is repressed by unknown mechanisms. The fact that CS activity is a few orders of magnitude higher than SAT activity in the amebae may explain why OAS was not detected under the normal conditions, but it does not explain why SMC is not synthesized. The observed increase in OAS under L-cysteine depletion also indicates that L-cysteine-sensitive SAT1 and SAT2 are derepressed (*i.e.* L-cysteine-mediated feedback inhibition of SAT1/2 was reversed) under L-cysteine depletion.

In addition to the feedback inhibition, the cysteine biosynthetic pathway is also regulated by the bi-enzyme complex of SAT and CS (47). This complex is not involved in the metabolic channeling of OAS from SAT to CS, because OAS freely diffuses out of the complex. The formation of the SAT·CS complex (cysteine synthase complex) was shown to modulate the kinetic parameters of both enzymes. It was shown that the complex was dissociated by the elevated OAS levels (47). It is possible that OAS affects the formation and dissociation of the cysteine synthase complex in *E. histolytica* and the SMC but not L-cysteine forming activity of the complex. Although OAS also acts as an inducer of the L-cysteine regulon in bacteria (48), the gene expression of SAT and CS isotypes was not affected upon L-cysteine depletion in *E. histolytica* (data not shown).

Role and Fate of SMC—Because genes encoding other enzymes that utilize methanethiol as a substrate, such as *O*-acetylhomoserine sulfhydrylase (EC 2.5.1.49) and methanethiol oxidase (EC 1.8.3.4), are absent in the *E. histolytica* genome (10), SMC synthesis is likely the major salvaging pathway of methanethiol. SMC is present in relatively large amounts in several legumes, and there are a few lines of evidence demonstrating that the methyl moiety of SMC is incorporated into various metabolites (methionine, choline, and creatine) and proteins (pectin) (37, 49–51). In plants (*e.g. Brassica pekinensis*), SMC can also be demethylated to generate L-cysteine (52). Metabolic labeling with SMC revealed that L-methionine and L-cysteine are formed from SMC in *Neurospora crassa* grown in low sulfur medium (53). In addition, methionine and cystathionine-auxotrophic mutants of *N. crassa* were able to grow when supplemented with SMC (53). Despite evidence from the studies, the fate of SMC in *E. histolytica* remains to be established because neither labeled L-cysteine nor L-methionine was detected using isotope-labeled serine in our metabolomic analysis. The role of methionine γ-lyase in *E. histolytica* could be to generate methanethiol for the synthesis of SMC. It has been shown in other organisms that the methyl and thiomethyl moieties of SMC are transferred to unidentified metabolites or proteins (49–53).

L-Cysteine Deprivation Affected SAM and Amino Acid Concentrations, Glycolysis, and Energy Generation—L-Cysteine depletion results in reduced levels of SAM, a precursor for polyamine biosynthesis and the essential methyl donor for numerous transmethylation reactions, including DNA methylation. This decrement in the SAM level is likely caused by either the reduction of SAM production by methionine adenosyltransferase or increased utilization of SAM. Because the amount of polyamines, such as putrescine, spermidine (supplemental Fig. S1), and *N*-acetylputrescine (data not shown), remained unchanged, SAM-dependent methylation may have increased upon L-cysteine deprivation. Because the methionine adenosyltransferase activity from various organisms is inhibited by nitric oxide-mediated nitrosylation of the cysteine residues in its active site (54), it is conceivable that methionine adenosyltransferase activity is inhibited by L-cysteine deprivation. The observed increase in L-threonine and L-serine can be attributed to their increased uptake, which is supported by the fact that L-cysteine is a strong inhibitor of L-threonine and L-serine uptake in the BSC-1 epithelial cell line (55).

Response of E. histolytica to L-Cysteine Depletion

We also demonstrated that L-cysteine deprivation repressed glycolysis and energy generation. Upon L-cysteine depletion, pyruvate and other upstream glycolytic intermediates accumulated that appeared to be rerouted toward the associated pathways. For example, the metabolites linked to pyruvate and phosphoenolpyruvate (*i.e.* alanine, malate, and fumarate), 3-phosphoglycerate (*i.e.* *O*-phosphoserine), and dihydroxyacetone-phosphate (*i.e.* Gly 3-P) increased in response to L-cysteine depletion. In contrast, the level of acetyl-CoA, ethanol, and the major nucleotide triphosphates significantly decreased. In *E. histolytica*, pyruvate is utilized by pyruvate:ferredoxin oxidoreductase, a highly oxygen-sensitive iron-sulfur cluster-containing protein (56). Our data are consistent with the premise that L-cysteine depletion-mediated oxidative stress inactivates pyruvate:ferredoxin oxidoreductase and other redox-sensitive enzymes, which results in the overall reduction in the glycolytic flux and the accumulation of upstream glycolytic intermediates. It has been shown in *E. histolytica* that under oxidative or nitrosative stress, pyruvate, glucose 6-phosphate, and fructose 6-phosphate accumulate, whereas ethanol and ATP decrease (33, 56). Unlike nitrosative stress, L-cysteine depletion for 48 h did not induce apoptosis (data not shown), and the decrease in ATP content appears to be primarily a result of the reduced glycolytic flux. Whole genome microarray analysis has revealed that L-cysteine depletion does not affect the expression of most of the genes involved in energy metabolism, with the exception of phosphoglycerate mutase and malate dehydrogenase, which were slightly down-regulated by 1.6- and 2.1-fold, respectively.[7] Down-regulation of these two genes may also contribute, at least in part, to the overall reduction in the glycolytic flux.

Discovery of Isopropanolamine and PtdIspn Synthesis upon L-Cysteine Deprivation—We have demonstrated for the first time that the Kennedy pathway, the major pathway for phospholipid biosynthesis, is regulated by the level of L-cysteine in *E. histolytica*. L-Cysteine deprivation resulted in the accumulation of an unusual phospholipid, PtdIspn, and also affected the composition and ratio of the major phospholipids. Under L-cysteine-depleted conditions, the synthesis of Ispn, Ispn-P, Etn-P, and Cho-P was elevated, PtdEtn synthesis was down-regulated, and the levels of Etn, Cho, PtdCho, phosphatidylserine, phosphatidylinositol, and phosphatidic acid were unaffected (Fig. 4).

Based on the findings related to phospholipid biosynthesis, we propose the following scheme for the involvement of L-cysteine. When *E. histolytica* is cultured under L-cysteine-depleted conditions, Ispn synthesis is increased. Ispn-P, formed from Ispn and ATP in a reaction catalyzed by Etn/Cho kinase (EHI_148580 (EAL52090.1); EHI_152340 (EAL51511.1)), then competes with Etn-P for Etn-P cytidyltransferase (EHI_095120 (EAL44415.1); EHI_140590 (EAL48799.1)), which appears to be the rate-limiting enzyme for the production of CDP-Ispn. This competition leads to an accumulation of Etn-P and a decrease in PtdEtn. The fact that PtdCho level was not affected by either L-cysteine depletion or Ispn supplementation, whereas Cho-P level increased upon L-cysteine depletion (Fig. 4*A*), suggests that Ispn-P does not compete with Cho-P for Etn-P/Cho-P cytidyltransferase. This observation also indicates that the increase in Cho-P is a consequence of increased production from accumulated Etn-P by SAM-dependent methylation, which may also contribute to the decrement in the SAM level. Alternatively, Ispn-P may compete with Cho-P for Etn-P/Cho-P cytidyltransferase, but the contribution of *de novo* synthesized PtdCho is negligible compared with the PtdCho incorporated from the culture milieu (Fig. 4).

Significance of PtdIspn Production upon L-Cysteine Deprivation—One of the consequences of the L-cysteine-dependent increase in Ispn synthesis is the concomitant increment in Etn-P, which is a known scavenger of free radicals (57). However, the increment of PtdIspn by L-cysteine depletion is not associated with either oxidative stress or changes in the redox status, because D-cysteine did not alleviate the PtdIspn synthesis, and paraquat/air treatment did not increase PtdIspn synthesis.

Similar to PtdEtn, phosphatidyl-propanolamine, an analog of PtdIspn, is a nonbilayer or hexagonal phase-forming phospholipid; however, it is not known whether PtdIspn is also similar to PtdEtn and phosphatidylpropanolamine in its nonbilayer or hexagonal phase-forming nature (58). Hexagonal phase-forming phospholipids have been proposed to be important for membrane fluidity, protein translocation, and membrane fusion events (59, 60). In PtdEtn methylation-defective mutants of *Saccharomyces cerevisiae*, supplementation of the culture medium with propanolamine leads to phosphatidylpropanolamine production and thus presumably compensates for the role of PtdCho and its *N*-methylated phospholipid precursors (58). However, mitochondrial PtdEtn cannot be completely replaced by phosphatidylpropanolamine, suggesting that PtdEtn is essential for the structure and function of mitochondrial membranes (58). It has been shown that changes in the PtdCho/PtdEtn ratio affect membrane integrity of large unilamellar vesicles in mouse hepatocytes, and this ratio is inversely correlated with leakage across the membrane (61). Because L-cysteine depletion also increases the PtdCho/PtdEtn ratio, it is conceivable that this changes membrane integrity and fluidity and affects protein translocation across the plasma membrane. In addition, because PtdEtn also plays various metabolic roles in cells, a decrease in PtdEtn level may also affect other cellular processes, including the synthesis of GPI anchors and protein modification.

To date, this is the first report to show that PtdIspn synthesis is increased by changes in environmental conditions. PtdIspn and phosphatidylpropanolamine have been identified in various organisms, including yeast, protozoa, and animals, and are considered to be unnatural phospholipids synthesized only under conditions where Ispn or propanolamine are supplied in the culture medium (58, 62) or administered intraperitoneally (63). Recently, PtdIspn has been shown to be naturally synthesized in BHK cells through the decarboxylation of the rare phospholipid phosphatidylthreonine (64).

[7] A. Husain, D. Sato, G. Jeelani, M. Suematsu, T. Soga, and T. Nozaki, unpublished data.

In conclusion, we have demonstrated that L-cysteine regulates various metabolic pathways in *E. histolytica* and thus affects the concentrations of the amino acids, phospholipids, and intermediary metabolites involved in central energy metabolism. Further investigation on the physiological role and fate of SMC and PtdIspn will help to better understand sulfur-containing amino acid metabolism, which is considered an attractive drug target for the development of new chemotherapeutics against this pathogen (18, 65). Future research is also needed to understand the function of PtdIspn in the plasma membrane and membrane-bound organelles and in the regulation of phospholipid metabolism.

Acknowledgments—We thank Takako Hishiki (Keio University) for the initial acquisition and analysis of CE-MS data and helpful discussions, Masahiro Sugimoto and Akiyoshi Hirayama (Keio University) for the use of CE-MS data analysis software (MasterHands), and all of the members of our laboratory for technical assistance and valuable discussions.

REFERENCES

1. Beinert, H., Holm, R. H., and Münck, E. (1997) *Science* **277,** 653–659
2. Stanley, S. L., Jr. (2003) *Lancet* **361,** 1025–1034
3. Weinbach, E. C., and Diamond, L. S. (1974) *Exp. Parasitol.* **35,** 232–243
4. Mehlotra, R. K. (1996) *Crit. Rev. Microbiol.* **22,** 295–314
5. Nozaki, T., Asai, T., Kobayashi, S., Ikegami, F., Noji, M., Saito, K., and Takeuchi, T. (1998) *Mol. Biochem. Parasitol.* **97,** 33–44
6. Clark, C. G., Alsmark, U. C., Tazreiter, M., Saito-Nakano, Y., Ali, V., Marion, S., Weber, C., Mukherjee, C., Bruchhaus, I., Tannich, E., Leippe, M., Sicheritz-Ponten, T., Foster, P. G., Samuelson, J., Noël, C. J., Hirt, R. P., Embley, T. M., Gilchrist, C. A., Mann, B. J., Singh, U., Ackers, J. P., Bhattacharya, S., Bhattacharya, A., Lohia, A., Guillén, N., Duchêne, M., Nozaki, T., and Hall, N. (2007) *Adv. Parasitol.* **65,** 51–190
7. Nozaki, T., Asai, T., Sanchez, L. B., Kobayashi, S., Nakazawa, M., and Takeuchi, T. (1999) *J. Biol. Chem.* **274,** 32445–32452
8. Nozaki, T., Ali, V., and Tokoro, M. (2005) *Adv. Parasitol.* **60,** 1–99
9. Hussain, S., Ali, V., Jeelani, G., and Nozaki, T. (2009) *Mol. Biochem. Parasitol.* **163,** 39–47
10. Loftus, B., Anderson, I., Davies, R., Alsmark, U. C., Samuelson, J., Amedeo, P., Roncaglia, P., Berriman, M., Hirt, R. P., Mann, B. J., Nozaki, T., Suh, B., Pop, M., Duchene, M., Ackers, J., Tannich, E., Leippe, M., Hofer, M., Bruchhaus, I., Willhoeft, U., Bhattacharya, A., Chillingworth, T., Churcher, C., Hance, Z., Harris, B., Harris, D., Jagels, K., Moule, S., Mungall, K., Ormond, D., Squares, R., Whitehead, S., Quail, M. A., Rabbinowitsch, E., Norbertczak, H., Price, C., Wang, Z., Guillén, N., Gilchrist, C., Stroup, S. E., Bhattacharya, S., Lohia, A., Foster, P. G., Sicheritz-Ponten, T., Weber, C., Singh, U., Mukherjee, C., El-Sayed, N. M., Petri, W. A., Jr., Clark, C. G., Embley, T. M., Barrell, B., Fraser, C. M., and Hall, N. (2005) *Nature* **433,** 865–868
11. Tokoro, M., Asai, T., Kobayashi, S., Takeuchi, T., and Nozaki, T. (2003) *J. Biol. Chem.* **278,** 42717–42727
12. Sato, D., Yamagata, W., Harada, S., and Nozaki, T. (2008) *FEBS J.* **275,** 548–560
13. Fahey, R. C., Newton, G. L., Arrick, B., Overdank-Bogart, T., and Aley, S. B. (1984) *Science* **224,** 70–72
14. Gillin, F. D., and Diamond, L. S. (1980) *J. Protozool.* **27,** 474–478
15. Gillin, F. D., and Diamond, L. S. (1981) *Exp. Parasitol.* **52,** 9–17
16. Gillin, F. D., and Diamond, L. S. (1981) *Exp. Parasitol.* **51,** 382–391
17. Jeelani, G., Husain, A., Sato, D., Ali, V., Suematsu, M., Soga, T., and Nozaki, T. (2010) *J. Biol. Chem.* **285,** 26889–26899
18. Ali, V., and Nozaki, T. (2007) *Clin. Microbiol. Rev.* **20,** 164–187
19. Soga, T., Baran, R., Suematsu, M., Ueno, Y., Ikeda, S., Sakurakawa, T., Kakazu, Y., Ishikawa, T., Robert, M., Nishioka, T., and Tomita, M. (2006) *J. Biol. Chem.* **281,** 16768–16776
20. Sato, S., Soga, T., Nishioka, T., and Tomita, M. (2004) *Plant J.* **40,** 151–163
21. Soga, T., Ohashi, Y., Ueno, Y., Naraoka, H., Tomita, M., and Nishioka, T. (2003) *J. Proteome Res.* **2,** 488–494
22. Diamond, L. S., Harlow, D. R., and Cunnick, C. C. (1978) *Trans. R. Soc. Trop. Med. Hyg.* **72,** 431–432
23. Clark, C. G., and Diamond, L. S. (2002) *Clin. Microbiol. Rev.* **15,** 329–341
24. Ohashi, Y., Hirayama, A., Ishikawa, T., Nakamura, S., Shimizu, K., Ueno, Y., Tomita, M., and Soga, T. (2008) *Mol. Biosyst.* **4,** 135–147
25. Soga, T., and Heiger, D. N. (2000) *Anal. Chem.* **72,** 1236–1241
26. Soga, T., Ueno, Y., Naraoka, H., Ohashi, Y., Tomita, M., and Nishioka, T. (2002) *Anal. Chem.* **74,** 2233–2239
27. Soga, T., Igarashi, K., Ito, C., Mizobuchi, K., Zimmermann, H. P., and Tomita, M. (2009) *Anal. Chem.* **81,** 6165–6174
28. Sugimoto, M., Wong, D. T., Hirayama, A., Soga, T., and Tomita, M. (2010) *Metabolomics* **6,** 78–95
29. Smith, C. A., Want, E. J., O'Maille, G., Abagyan, R., and Siuzdak, G. (2006) *Anal. Chem.* **78,** 779–787
30. Baran, R., Kochi, H., Saito, N., Suematsu, M., Soga, T., Nishioka, T., Robert, M., and Tomita, M. (2006) *BMC Bioinformatics* **7,** 530
31. Bai, J., Rodriguez, A. M., Melendez, J. A., and Cederbaum, A. I. (1999) *J. Biol. Chem.* **274,** 26217–26224
32. Aceti, D. J., and Ferry, J. G. (1988) *J. Biol. Chem.* **263,** 15444–15448
33. Ramos-Martínez, E., Olivos-García, A., Saavedra, E., Nequiz, M., Sánchez, E. C., Tello, E., El-Hafidi, M., Saralegui, A., Pineda, E., Delgado, J., Montfort, I., and Pérez-Tamayo, R. (2009) *Int. J. Parasitol.* **39,** 693–702
34. Bligh, E. G., and Dyer, W. J. (1959) *Can. J. Biochem. Physiol.* **37,** 911–917
35. Zhou, X., and Arthur, G. (1992) *J. Lipid Res.* **33,** 1233–1236
36. Rébeillé, F., Jabrin, S., Bligny, R., Loizeau, K., Gambonnet, B., Van Wilder, V., Douce, R., and Ravanel, S. (2006) *Proc. Natl. Acad. Sci. U.S.A.* **103,** 15687–15692
37. Giovanelli, J., Mudd, S. H., and Datko, A. H. (1980) in *The Biochemistry of Plants* (Miflin B. J., eds.), Vol. 5, pp. 453–487, Academic Press, New York
38. Zuo, X., and Coombs, G. H. (1995) *FEMS Microbiol. Lett.* **130,** 253–258
39. Husain, A., Jeelani, G., Sato, D., Ali, V., and Nozaki, T. (2010) *Mol. Biochem. Parasitol.* **170,** 100–104
40. Anderson, I. J., and Loftus, B. J. (2005) *Exp. Parasitol.* **110,** 173–177
41. Kelley, J. J., and Dekker, E. E. (1984) *J. Biol. Chem.* **259,** 2124–2129
42. Green, M. L., and Elliott, W. H. (1964) *Biochem. J.* **92,** 537–549
43. Ray, M., and Ray, S. (1987) *J. Biol. Chem.* **262,** 5974–5977
44. Inoue, Y., and Kimura, A. (1995) *Adv. Microb. Physiol.* **37,** 177–227
45. Westrop, G. D., Goodall, G., Mottram, J. C., and Coombs, G. H. (2006) *J. Biol. Chem.* **281,** 25062–25075
46. Ariyanayagam, M. R., and Fairlamb, A. H. (1999) *Mol. Biochem. Parasitol.* **103,** 61–69
47. Wirtz, M., Birke, H., Heeg, C., Mueller, C., Hosp, F., Throm, C., Koenig, S., Feldman-Salit, A., Rippe, K., Petersen, G., Wade, R. C., Rybin, V., Scheffzek, K., and Hell, R. (2010) *J. Biol. Chem.* **285,** 32810–32817
48. Kredich, N. M. (1992) *Mol. Microbiol.* **6,** 2747–2753
49. Horner, W. H., and Kuchinskas, E. J. (1959) *J. Biol. Chem.* **234,** 2935–2937
50. Ronald, C. D., and John, F. T. (1971) *Phytochemistry* **10,** 1745–1750
51. Mae, T., and Ohira, K. (1976) *Plant Cell Physiol.* **17,** 459–465
52. Mae, T., Ohira, K., and Fujiwara, A. (1971) *Plant Cell Physiol.* **12,** 881–887
53. Wiebers, J. L., and Garner, H. R. (1964) *J. Bacteriol.* **88,** 1798–1804
54. Pérez-Mato, I., Castro, C., Ruiz, F. A., Corrales, F. J., and Mato, J. M. (1999) *J. Biol. Chem.* **274,** 17075–17089
55. Kuhlmann, M. K., and Vadgama, J. V.(1991) *J. Biol. Chem.* **266,** 15042–15047
56. Ramos, E., Olivos-García, A., Nequiz, M., Saavedra, E., Tello, E., Saralegui, A., Montfort, I., and Pérez Tamayo, R. (2007) *Exp. Parasitol.* **116,** 257–265
57. Gordon, L. I., Weiss, D., Prachand, S., and Weitzman, S. A. (1991) *Free Radic. Res. Commun.* **15,** 65–71
58. Choi, J. Y., Martin, W. E., Murphy, R. C., and Voelker, D. R. (2004)

J. Biol. Chem. **279,** 42321–42330
59. Yeagle, P. L. (1989) *FASEB J.* **3,** 1833–1842
60. Cullis, P. R., Fenske, D. B., and Hope, M. J. (1996) in *Biochemistry of Lipids, Lipoproteins and Membranes* (Vance, D. E., and Vance, J., eds) Vol. 31, pp. 1–33, Elsevier, Paris
61. Li, Z., Agellon, L. B., Allen, T. M., Umeda, M., Jewell, L., Mason, A., and Vance, D. E. (2006) *Cell Metab.* **3,** 321–331
62. Smith, J. D., and Barrows, L. J. (1988) *Biochem. J.* **254,** 301–302
63. Meyer, W., Wahl, R., and Gercken, G. (1979) *Biochim. Biophys. Acta* **575,** 463–466
64. Heikinheimo, L., and Somerharju, P. (2002) *Traffic* **3,** 367–377
65. Sato, D., Kobayashi, S., Yasui, H., Shibata, N., Toru, T., Yamamoto, M., Tokoro, G., Ali, V., Soga, T., Takeuchi, T., Suematsu, M., and Nozaki, T. (2010) *Int. J. Antimicrob. Agents* **35,** 56–61

THE JOURNAL OF BIOLOGICAL CHEMISTRY VOL. 285, NO. 35, pp. 26889–26899, August 27, 2010

Two Atypical L-Cysteine-regulated NADPH-dependent Oxidoreductases Involved in Redox Maintenance, L-Cystine and Iron Reduction, and Metronidazole Activation in the Enteric Protozoan *Entamoeba histolytica*[*] [S]

Received for publication, January 24, 2010, and in revised form, June 28, 2010 Published, JBC Papers in Press, June 30, 2010, DOI 10.1074/jbc.M110.106310

Ghulam Jeelani[‡§1], Afzal Husain[‡], Dan Sato[¶], Vahab Ali[‖], Makoto Suematsu[**], Tomoyoshi Soga[¶], and Tomoyoshi Nozaki[‡1,2]

From the [‡]Department of Parasitology, National Institute of Infectious Diseases, 1-23-1 Toyama, Shinjuku-ku, Tokyo 162-8640, Japan, the [§]Center for Integrated Medical Research, School of Medicine, Keio University, Shinjuku, Tokyo 160-8582, Japan, the [¶]Institute for Advanced Biosciences, Keio University, Tsuruoka, Yamagata 997-0052, Japan, the [‖]Department of Biochemistry, Rajendra Memorial Research Institute of Medical Sciences, Agamkuan, Patna-800007, India, and the [**]Department of Biochemistry and Integrative Medical Biology, School of Medicine, Keio University, Shinjuku, Tokyo 160-8582, Japan

We discovered novel catalytic activities of two atypical NADPH-dependent oxidoreductases (EhNO1/2) from the enteric protozoan parasite *Entamoeba histolytica*. EhNO1/2 were previously annotated as the small subunit of glutamate synthase (glutamine:2-oxoglutarate amidotransferase) based on similarity to authentic bacterial homologs. As *E. histolytica* lacks the large subunit of glutamate synthase, EhNO1/2 were presumed to play an unknown role other than glutamine/glutamate conversion. Transcriptomic and quantitative reverse PCR analyses revealed that supplementation or deprivation of extracellular L-cysteine caused dramatic up- or down-regulation, respectively, of EhNO2, but not EhNO1 expression. Biochemical analysis showed that these FAD- and 2[4Fe-4S]-containing enzymes do not act as glutamate synthases, a conclusion which was supported by phylogenetic analyses. Rather, they catalyze the NADPH-dependent reduction of oxygen to hydrogen peroxide and L-cystine to L-cysteine and also function as ferric and ferredoxin-$NADP^+$ reductases. EhNO1/2 showed notable differences in substrate specificity and catalytic efficiency; EhNO1 had lower K_m and higher k_{cat}/K_m values for ferric ion and ferredoxin than EhNO2, whereas EhNO2 preferred L-cystine as a substrate. In accordance with these properties, only EhNO1 was observed to physically interact with intrinsic ferredoxin. Interestingly, EhNO1/2 also reduced metronidazole, and *E. histolytica* transformants overexpressing either of these proteins were more sensitive to metronidazole, suggesting that EhNO1/2 are targets of this anti-amebic drug. To date, this is the first report to demonstrate that small subunit-like proteins of glutamate synthase could play an important role in redox maintenance, L-cysteine/L-cystine homeostasis, iron reduction, and the activation of metronidazole.

Glutamate synthase (glutamine:2-oxoglutarate amidotransferase, GOGAT[3]) is an iron sulfur flavoprotein that catalyzes the transfer of the amide group of L-glutamine to 2-oxoglutrate to yield L-glutamate and is a key enzyme in the nitrogen assimilation pathway. In eubacteria, this enzyme is dependent on the pyridine nucleotide NAD(P)H for its reducing equivalents and is composed of large 150-kDa (α) and small 50-kDa (β) subunits that together form the active $\alpha\beta$ protomer (1). The structural genes encoding the α and β subunit polypeptides are commonly designated *gltB* and *gltD*, respectively, and lie adjacent on the chromosome with the α subunit preceding the β subunit, except in γ-proteobacteria, where the gene order is reversed. The small subunit of eubacterial glutamate synthase shows sequence similarity to several other protein domains and enzyme subunits (2, 3) and is, therefore, proposed to represent a prototype domain used in many different cellular processes to transfer electrons from NAD(P)H to an acceptor protein or protein domain of unknown function (4). In concord with this view, numerous organisms have been recently identified to possess glutamate synthase β subunit-like genes based on DNA sequence homology (4, 5); however, the organisms often lack a gene encoding the corresponding α subunit, or the β subunit is not present adjacent to the α subunit and is, therefore, transcribed independently (5, 6). To our knowledge, among the organisms lacking a putative GOGAT α subunit, only the GOGAT β subunit from *Thermococcus kodakaraensis* (renamed from *Pyrococcus* sp. KOD1) has been functionally associated with independent GOGAT activity (7).

* This work was supported by Grants-in-aid for Scientific Research 18GS0314, 18050006, and 18073001 (to T. N.) from the Ministry of Education, Culture, Sports, Science, and Technology of Japan, a grant for research on emerging and re-emerging infectious diseases from the Ministry of Health, Labour, and Welfare of Japan (H20-Shinkosaiko-016), and a grant for research to promote the development of anti-AIDS pharmaceuticals from the Japan Health Sciences Foundation (to T. N.).

[S] The on-line version of this article (available at http://www.jbc.org) contains supplemental Figs. S1–S3.

The nucleotide sequence(s) reported in this paper has been submitted to the GenBank™/EBI Data Bank with accession number(s) AB521132 and AB521133.

[1] Supported in part by the Global Center of Excellence Program for Human Metabolomic System Biology of the Ministry of Education Culture, Sports, Science, and Technology.

[2] To whom correspondence should be addressed. Tel.: 81-3-5285-1111 (ext. 2600); Fax.: 81-3-5285-1219; E-mail: nozaki@nih.go.jp.

[3] The abbreviations used are: GOGAT, glutamine:2-oxoglutarate amidotransferase; EhNO, *E. histolytica* NADPH-dependent oxidoreductase; rEhNO, recombinant EhNO; INT, iodonitrotetrazolium; CE, capillary electrophoresis; SoFd, *S. oleracea* ferredoxin; EhFd1, *E. histolytica* ferredoxin.

Entamoeba histolytica, the causative agent of human amebiasis, is an enteric protozoan parasite responsible for amebic colitis and extraintestinal abscesses in approximately 50 million inhabitants of endemic areas (8). As is the case with other microaerophilic parasitic infections, such as giardiasis and trichomoniasis, the 5-nitroimidazole drug metronidazole has been established as the most effective treatment of amebiasis. Because of the high prevalence of these infections (9) and because of its role as a second-line defense against *Helicobacter pylori* infections (10), metronidazole has been included in the list of "essential medicines" by the World Health Organization (11). Metronidazole is a prodrug that requires reduction of the nitro group to generate the cytotoxic nitroradical anion that undergoes further reduction resulting in the generation of nitrosoimidazole (12, 13). This active form can then react with sulfhydryl groups (14) and DNA (15) while being further reduced to an amine via a hydroxylamine intermediate. Here, we report for the first time multiple novel roles of two GOGAT β subunit-like proteins in *E. histolytica*. We demonstrated that they are not associated with glutamate synthase activity but instead exhibit robust reductase activities against L-cystine, ferredoxin, and ferric ion and are also involved in the response to oxidative stress. In addition, we showed that these enzymes can be capable of reducing and activating metronidazole and, thus, are responsible for its observed toxicity against *E. histolytica*. We designated the novel NADPH-dependent oxidoreductases as EhNO1 and -2.

EXPERIMENTAL PROCEDURES

Chemicals and Reagents—L-Cysteine, L-cystine, *trans*-epoxysuccinyl-L-leucylamido-(4-guanidino) butane, cytochrome *c*, iodonitrotetrazolium (INT), and metronidazole were purchased from Sigma. Nickel-nitrilotriacetic acid-agarose was purchased from Merck. All other chemicals of analytical grade were purchased from Wako Pure Chemical (Osaka, Japan) unless otherwise stated.

Microorganisms and Cultivation—Trophozoites of the *E. histolytica*, clonal strain HM1:IMSS cl 6 were maintained axenically in Diamond's BI-S-33 medium at 35.5 °C as described previously (16, 17). Trophozoites were harvested in the late logarithmic growth phase for 2–3 days after inoculation of 1/30 to 1/12 of the total culture volume. After the cultures were chilled on ice for 5 min, trophozoites were collected by centrifugation at 500 × *g* for 10 min at 4 °C and washed twice with ice-cold PBS (pH 7.4). *Escherichia coli* BL21 (DE3) strain was purchased from Invitrogen.

Quantitative Real-time PCR—Trophozoites were cultured in BI-S-33 medium supplemented with or without 10 mM L-cysteine (18 or 8 mM final, respectively). After placing the culture on ice for 5 min, the trophozoites were harvested by centrifugation at 500 × *g* for 5 min at 4 °C. Polyadenylated RNA was extracted from ~6 × 10^6 tropozoites with an mRNA isolation kit (Stratagene, La Jolla, CA) and then treated with deoxyribonuclease I (Invitrogen). cDNA was reverse-transcribed with 4 μg of isolated polyadenylated RNA, the SuperScript III First-Strand Synthesis System, and an oligo$(dT)_{20}$ primer (Invitrogen). PCR was performed with the resulting cDNA as a template and specific oligonucleotide primers using the ABI PRISM 7300 Sequence Detection System (Applied Biosystems, Japan). The primers used were 5′-AGCTGCACCAGTTCCAATTC-3′ and 5′-CAATCCCCAGCTGCATATAA-3′ (EhNO1), 5′-CAGTTCCAATTCCAGGCAGT-3′ and 5′-TTGGTCCTGTAACACAATCTCCT-3′ (EhNO2), and 5′-GATCCAACATATCCTAAAACAACA-3′ and 5′-TCAATTATTTTCTGACCCGTCTTC-3′ (RNA polymerase II 15-kDa subunit, GenBank™ accession number XM_643999). The parameters for PCR were as follows: an initial step of denaturation at 95 °C for 9 min followed by 40 cycles of denaturation at 94 °C for 30 s, annealing at 50 °C for 30 s, and extension at 65 °C for 1 min and a final step at 95 °C for 9 s, 60 °C for 9 s, and 95 °C for 9 s was used to remove primer dimers.

Amino Acid Comparison and Phylogenetic Analysis—Amino acid sequences of the GOGAT β subunit and β subunit-like proteins from 40 other organisms were obtained from the DDBJ/EBI/GenBank™ data base using BLASTP searches with the novel amebic NADPH-dependent oxidoreductases (EhNO1 and EhNO2) described in this paper as queries. Sequence alignments of these proteins were generated using the ClustalW program (18). The alignments obtained by ClustalW were inspected and manually corrected using the Genedoc program (19). After the removal of all gaps, 326 unambiguously aligned residues were selected for phylogenetic analyses. The neighbor-joining and maximum parsimony methods were used to construct a final phylogenetic tree for 32 sequences using the MEGA4.1 program (20). The branch lengths and bootstrap values of 1000 replicates (in percentage) in these trees were obtained from the neighbor-joining analysis.

Construction of Plasmids—Standard techniques were used for cloning and plasmid construction, as previously described (21). Genes encoding EhNO1 and EhNO2 were cloned to produce a fusion protein containing a histidine tag (provided by the vector) at the amino terminus. The cDNA corresponding to the open reading frames of EhNO1 and EhNO2 was amplified by PCR using an *E. histolytica* cDNA library (22) as a template and oligonucleotide primers. The sense and antisense oligonucleotide primers used to amplify EhNO1 and EhNO2 were 5′-CTTATAA**GGATCC**ATGAAGAGTTTCAACATTA-3′ and 5′-ATA**GTCGAC**TTAATCTTGTTCCATTGGG-3′ (EhNO1) and 5′-CTTATAA**GGATCC**ATGGCTGCTAATTATAATA-3′ and 5′-ATA**GTCGAC**TTATTCTTCATTTTTTTTACCC-3′ (EhNO2) (bold letters indicate BamHI and SalI restriction sites). PCR was performed with Platinum *Pfx* DNA polymerase (Invitrogen) and the following parameters: an initial incubation at 94 °C for 2 min followed by 30 cycles of denaturation at 94 °C for 15 s, annealing at 45 °C for 30 s, and elongation at 68 °C for 2 min and a final extension at 68 °C for 10 min. The PCR fragments were digested with BamHI and SalI, subjected to gel electrophoresis, excised, purified with the Gene clean kit II (BIO 101, Vista, CA), and then ligated into BamHI- and SalI-digested pCOLD I (Takara Bio, Otsu, Japan) in the identical orientation as the T7 promoter to generate pCOLD1-EhNO1 and pCOLD1-EhNO2. The nucleotide sequences of the cloned EhNO1 and EhNO2 genes were verified by sequencing to be identical to the putative protein coding

regions of XP_656997 and XP_653573, respectively, in *E. histolytica*.

Bacterial Expression and Purification of Recombinant EhNO (rEhNO)—The pCOLD1-EhNO1 and pCOLD1-EhNO2 expression constructs were introduced into competent *E. coli* BL21 (DE3) cells by heat shock at 42 °C for 30 s, and the resulting transformants were grown at 37 °C in 100 ml of Luria Bertani medium in the presence of 50 μg/ml ampicillin. The overnight culture was then used to inoculate 500 ml of fresh medium, which was further cultured at 37 °C with shaking at 180 rpm. When the A_{600} reached 0.6, 1 mM isopropyl β-D-thiogalactopyranoside was added to induce protein expression, and cultivation was continued for 24 h at 15 °C. The *E. coli* cells were then harvested by centrifugation at 4050 × *g* for 20 min at 4 °C, and the resulting cell pellet was washed with PBS (pH 7.4) and re-suspended in 20 ml of lysis buffer (50 mM Tris-HCl (pH 8.0), 300 mM NaCl, and 10 mM imidazole) containing 0.1% Triton X-100 (v/v), 100 μg/ml lysozyme, and 1 mM phenylmethylsulfonyl fluoride. After a 30-min incubation at room temperature, the cells were sonicated on ice and centrifuged at 25,000 × *g* for 15 min at 4 °C. The supernatant was mixed with 1.2 ml of a 50% nickel-nitrilotriacetic acid His-bind slurry (Qiagen, Tokyo, Japan) and incubated for 1 h at 4 °C with gentle shaking. The rEhNO-bound resin was washed three times with buffer A (50 mM Tris-HCl (pH 8.0), 300 mM NaCl, and 0.1% Triton X-100, v/v) containing 10–50 mM imidazole, and bound proteins were then eluted with buffer A containing 100–300 mM imidazole. After the integrity and purity of the rEhNO proteins were confirmed by 12% SDS-PAGE analysis and Coomassie Brilliant Blue staining, they were extensively dialyzed twice against a 300-fold volume of 50 mM Tris-HCl, 150 mM NaCl, pH 8.0, containing 10% glycerol (v/v) and the Complete Mini Protease Inhibitor Mixture (Roche Applied Science) for 18 h at 4 °C. The concentrations of the dialyzed proteins were spectrophotometrically determined by the Bradford method using bovine serum albumin as a standard as previously described (23). The rEhNO proteins were stored at −80 °C in 20% glycerol in small aliquots until needed.

Analysis of Prosthetic Groups—UV-visible absorption spectra of rEhNO1 (400 μg) and rEhNO2 (200 μg) were measured under both non-reducing and sodium dithionite-reducing conditions. The purified recombinant proteins were reduced with a 10-fold molar excess of sodium dithionite in 200 μl. Flavin was liberated from the recombinant enzymes by boiling samples for 10 min and then separated from proteins by centrifugation at 14,000 × *g* for 10 min. To determine whether FAD or FMN formed a prosthetic group, the fluorescence with excitation and emission wavelengths of 450 and 535 nm, respectively, was measured at pH 2.6 and 7.7 according to the method of Faeder and Siegel (24) using a fluorescence spectrophotometer (model F-2500; Hitachi).

Iron Assay—The iron content of EhNOs was determined by the *O*-phenanthroline method as previously described (25). Briefly, 60 μl samples of rEhNO1 and rEhNO2 were mixed with 4 μl of concentrated HCl and then diluted with distilled water to 0.2 ml. After the resulting mixtures were heated to 80 °C for 10 min and cooled to room temperature, they were then mixed with 0.6 ml of water, 40 μl of 10% hydroxylamine hydrochloride, and 0.2 ml of 0.1% *O*-phenanthroline and further incubated at room temperature for 30 min. The absorbances at 512 nm (A_{512}) were then measured, and the iron concentrations were determined by comparison to a standard curve generated with 0–100 μM ferrous sulfate.

Enzyme Assays—Glutamate synthase activity was assayed spectrophotometrically by measuring the rate of NADPH or NADH oxidation at 340 nm with slight modifications of the procedure described by Jongsareejit *et al.* (7). The 200-μl assay mixture contained 20 mM potassium phosphate buffer, pH 7.5, 5 mM concentrations each of L-glutamine and 2-oxoglutarate, 0.4 mM cofactor (NADPH or NADH), and varying concentrations of rEhNO proteins. The reaction was initiated by the addition of cofactor and was performed at 37 °C. To test for ammonia-dependent activity, glutamine was replaced with 100 mM NH_4Cl.

Oxidoreductase Activity—The NADPH-dependent reduction of menadione was monitored in a coupling assay under aerobic conditions. The rate of reduction of cytochrome *c* by menadione was monitored by the absorbance at 550 nm (ϵ_{550} = 21.1 mM^{-1} cm^{-1}). Measurements were made in 50 mM Tris-HCl (pH 7.5), 200 μM NADPH, 1 μM menadione, and 30 μM cytochrome *c*. The reactions were initiated by the addition of 2 μg of rEhNO1/2.

For the other electron acceptors tested, a standard mixture containing 0.1 mM NADPH, 50 mM Tris-HCl (pH 7.5), and either 0.5 mM INT, 1 mM potassium ferricyanide, or 10 mM paraquat was used. The reactions were initiated by the addition of 2 μg of rEhNO1/2 enzyme, and the reduction of the acceptors was monitored spectrophotometrically at 490 nm for INT (ϵ = 18.5 mM^{-1} cm^{-1}), 410 nm for potassium ferricyanide (ϵ = 1 mM^{-1} cm^{-1}), and 340 nm for paraquat (NADPH oxidation, ϵ = 6.22 mM^{-1} cm^{-1}). One unit of enzyme activity was defined as the formation of 1 μmol of product/min/mg of protein.

Metronidazole reduction activity was determined by measuring the oxidation of NADPH at 340 nm (ϵ_{340} = 6.22 mM^{-1} cm^{-1}) or the reduction of metronidazole at 360 nm (ϵ_{360} = 9.2 mM^{-1} cm^{-1}), as described by Chen and Blanchard (26). Assays were conducted at room temperature under strict anaerobic conditions. The reactions were initiated by the addition of 2 μg of rEhNO protein to a mixture comprising 50 mM Tris-HCl (pH 8.0), 0.5 mM metronidazole, and 0.2 mM NADPH.

The cystine reductase activity was calculated as μmol of NADPH oxidized per min at 340 nm. The assay mixture contained 0.1 M potassium phosphate (pH 7.5), 2 mM EDTA, 0.05–0.2 mM NADPH, and 0.1–5 mM L-cystine. Approximately 2 μg of rEhNO1/2 was added to initiate the reaction, and the change in absorbance at 340 nm was monitored. The effects of sulfydryl-dependent inhibitors were examined by preincubation of 2 μg of rEhNO1 and rEhNO2 with 0.1–5 mM *N*-ethylmaleimide for 10 min before the various assays. All sample reactions were performed in triplicate at a minimum.

NAD(P)H:flavin oxidoreductase activity was assayed by measuring the initial rate of NAD(P)H oxidation at 340 nm (ϵ = 6.22 $mM^{-1}cm^{-1}$) at 25 °C as described by Lo and Reeves (27). One unit of NAD(P)H:flavin oxidoreductase activity was defined as the amount of enzyme that catalyzed the oxidation of 1 μmol of NAD(P)H/min.

Ferric reductase activity was determined by measuring the difference of NAD(P)H consumption at 340 nm in the presence and absence of Fe(III) ammonium citrate. Reaction mixtures containing 0.2 mM NADPH, 100 mM Tris-HCl (pH 7.5), 0.005–1 mM ferric ammonium citrate, and 2 μg of rEhNO1 and -2 were used for the assays.

Ferredoxin-$NADP^+$ reductase activity was determined by measuring ferredoxin-dependent reduction of cytochrome *c* (28). Activity was measured by monitoring cytochrome *c* reduction at 550 nm ($\epsilon = 21.1\ mM^{-1}\ cm^{-1}$) in a reaction mixture containing 0.1 mM NADPH, 0.01–0.5 μM ferredoxin, 10 μM cytochrome *c*, and 50 mM Tris-HCl buffer (pH 7.5). The reactions were initiated by the addition of 1 μg of rEhNO1 and -2.

Determination of H_2O_2 Formation—The ferrithiocyanate method (29) was used to measure H_2O_2 formation at various time points (1–30 min) during the NADPH:favin oxidoreductase reaction. After the reactions were terminated by the addition of 0.125 volumes of 50% trichloroacetic acid, the samples were centrifuged at 12,000 × *g*, and 0.2 volumes of 10 mM ferrous ammonium sulfate and 0.1 volumes of 2.5 M potassium thiocyanate were then added. In the presence of H_2O_2, Fe^{2+} is oxidized, resulting in a colored thiocyanate-Fe^{3+} complex that can be measured by its absorption at 480 nm. The quantity of H_2O_2 formed was determined by comparison of the A_{480} values to standard curves generated using known amounts of H_2O_2.

Metabolite Extraction—Approximately 1.5 × 10^6 *E. histolytica* cells were harvested after 48 h of cultivation and washed twice with 5% mannitol. The cells were then resuspended in 1.6 ml of methanol containing 20 μM concentrations of the internal standard methionine sulfone acid and mixed with 1.6 ml of chloroform and 640 μl of deionized water. After vortexing, the mixture was centrifuged at 4600 × *g* at 4 °C for 5 min, and the aqueous layer (1.6 ml) was filtrated using an Amicon Ultrafree-MC ultrafilter (Corporation, Billerica, MA) by centrifugation at 9100 × *g* at 4 °C for ~2 h. The filtrate was dried and preserved at −80 °C until mass spectrometric analysis.

Instrumentation and Capillary Electrophoresis (CE)-Time of Flight Mass Spectrometry (TOFMS) Conditions—CE-TOFMS was carried out using an Agilent CE Capillary Electrophoresis System equipped with an Agilent 6210 Time-of-Flight mass spectrometer, Agilent 1100 isocratic HPLC pump, Agilent G1603A CE-MS adapter kit, and Agilent G1607A CE-ESI-MS sprayer kit (Agilent Technologies, Waldbronn, Germany). The system was controlled by Agilent G2201AA ChemStation software for CE. Data acquisition was performed by Analyst QS Build: 7222 software for Agilent TOF (Applied Biosystems/MDS Sciex, Ontario, Canada). Instrumental conditions for the separation and detection of metabolites were as follows. The metabolites were separated on a fused silica capillary (50 μm × 100 cm) using 1 M formic acid as the electrolyte, and the applied voltage was set at +30 kV. A solution of 50% (v/v) methanol-water was delivered as the sheath liquid at 10 μl/min (30, 31). Electrospray ionization-TOFMS was conducted in the positive ion mode (4000 V). The pressure of dry nitrogen gas was maintained at 10 p.s.i. Exact mass data were acquired over a 50–1000 *m/z* range (32, 33). Before analysis, the sample was dissolved in 20 μl of deionized water containing 200 μM concentrations of the internal standard 3-aminopyrrolidine.

Generation of E. histolytica Transformants Overexpressing EhNO—The protein coding regions of EhNO1 and EhNO2 were amplified by PCR from cDNA using sense and antisense oligonucleotides containing appropriate restriction sites at the 5′ end. The sense and antisense oligonucleotide primers used for EhNO1 and EhNO2 were 5′-CTA**CCCGGG**ATGAAGAG-TTTCAACATTACA-3′ and 5′-CAA**CTCGAG**TTAATCTT-GTTCCATTGGGGT-3′ (EhNO1) and 5′-CTA**CCCGGG**AT-GGCTGCTAATTATAATAGA-3′ and 5′-CAA**CTCGAG**TT-ATTCATTTTTTTTACC-3′ (EhNO2) (bold letters indicate restriction sites). The PCR-amplified DNA fragments were digested with SmaI and XhoI and ligated into SmaI and XhoI sites of the expression vector pKT-MR (34) to produce pKT-MR-NO1 and pKT-MR-NO2. Wild-type trophozoites were transformed with pKT-MR by liposome-mediated transfection as previously described (35). Transformants were initially selected in the presence of 3 μg/ml Geneticin (Invitrogen), which was then gradually increased to 6–20 μg/ml during the subsequent 2 weeks before subjecting the transformants to analyses.

Assay for Metronidazole Sensitivity of E. histolytica Trophozoites—To determine sensitivity to metronidazole, *E. histolytica* transfectants harboring pKT-MR-NO1, pKT-MR-NO2, or pKT-MR (control) were cultured at 37 °C in BI-S-33 medium containing 20 μg/ml Geneticin. For the assay, varying concentrations (0–16 μM) of metronidazole were added to samples containing an initial density of 10^4 cells/ml. After 48 h, the number of viable cells was counted on a hemocytometer using trypan blue to identify dead cells. The assays were performed five times in duplicate.

In Vitro Interaction of EhNO1/2 with Ferredoxin—Protein cross-linking was performed as described previously (36). Briefly, EhNO1/2 and ferredoxin (4 and 20 μM, respectively) were cross-linked by treatment with 5 mM *N*-ethyl-3-(3-dimethylaminopropyl)carbodiimide in 25 mM sodium phosphate, pH 7.5. The resulting complexes were analyzed by SDS-PAGE and Western blotting using anti-His antibody.

Immunoblot Analysis—Cell lysates and culture supernatants were separated on 12% (w/v) SDS-PAGE gels and subsequently electro-transferred onto nitrocellulose membranes (Hybond-C Extra; Amersham Biosciences) as previously described (37). Nonspecific binding was blocked by incubating the membranes for 1.5 h at room temperature in 5% nonfat dried milk in TBST (50 mM Tris-HCl (pH 8.0), 150 mM NaCl, and 0.05% Tween 20). The blots were then reacted with primary antibodies specific for EhNO1 and EhNO2 and mannose 6-phosphate receptor 1 (38) and cysteine synthase 1 (22) as controls for the membrane and cytosolic fractions, respectively, at dilutions of 1:500 to 1:100. Antisera against purified rEhNO1 and rEhNO2 were raised in rabbits commercially (Operon, Tokyo, Japan). The membranes were washed with TBST and further reacted with horseradish peroxidase-conjugated anti-rabbit or anti-mouse IgG antisera (1:20,000) (Invitrogen) at room temperature for 1.5 h. After further washing with TBST, specific proteins were visualized and measured with a chemiluminescence detection

system (Millipore) using Scion Image software (Scion Corp., Frederick, MD) (39).

RESULTS

Identification of a GOGAT Small β Subunit Gene in E. histolytica upon L-Cysteine Supplementation—Upon analysis of the transcriptome of *E. histolytica* trophozoites cultured in medium supplemented with L-cysteine, a highly up-regulated gene (XM_648481) was previously identified.[4] Although the entire transcriptome data is described elsewhere, we attempted to characterize this gene in detail in the present study. The identified gene and a gene (XM_651905) that appeared to be very closely related in the *E. histolytica* genome data base (40) were predicted to encode proteins showing high similarity to the small β subunit of GOGAT from bacteria. The genes were designated as *E. histolytica* NADPH-dependent oxidoreductase 1 and 2 [EhNO1 (XM_651905) and EhNO2 (XM_648481)] because although the encoded proteins lacked glutamate synthase activity, they showed robust NADPH-dependent oxidoreductase activity (described below). The EhNO1 and EhNO2 genes consisted of 1347- and 1338-bp open reading frames, respectively, which were predicted to encode proteins of 448 and 445 amino acids with predicted molecular masses of 49.3 and 49.0 kDa and isoelectric points of 6.31 and 7.02, respectively.

Features of the Deduced Protein Sequence of EhNOs—The predicted amino acid sequences of the two EhNOs shared 80% mutual identity and demonstrated 20–60% identities to the small β subunit of GOGAT from Archaea, bacteria, animals, and plants. EhNO1 had the highest amino acid identities to the GOGAT β subunit-like proteins of *Chlorobium tepidum* (green sulfur bacteria) and *Methanosarcina mazei* (Archaea) (62 and 59%, respectively), whereas EhNO2 showed 61–62% identities to the small subunit of *Pyrococcus abyssi* GOGAT and the β subunit chain of formate dehydrogenase from *Moorella thermoacetica* (Archaea). Although a multiple alignment of 32 GOGAT and GOGAT-like sequences was generated using ClustalW, the comparisons of representative sequences from *E. coli*, *Clostridium saccharobutylicum*, *Azospirillum brasilense*, and *E. histolytica* were sufficient to highlight the important similarities and differences among GOGAT proteins from these organisms and between the two EhNO isotypes (supplemental Fig. S1).

All of the functional domains characteristic of GOGAT β subunits were conserved between these β subunit-like proteins (supplemental Fig. S1). Two amino-terminal cysteine clusters, $CX_2CX_4CX_3CP$ (residues 40–53 for EhNO1 and residues 41–54 for EhNO2) and $CX_3CX_3CX_3C$ (residues 87–99, EhNO1; 88–100, EhNO2), matched the conserved cysteine-rich patterns proposed to be involved in the formation of [4Fe-4S] clusters (2). Similarly, two regions (residues 137–165 and 264–293 of EhNO1, labeled "FAD-I" and "NAD(P)H", respectively) matched the conserved sequences of an ADP binding fold for the binding of FAD and NAD(P)H. Both EhNO1 and -2 shared features in the NAD(P)H binding domain with the *A. brasilense* GOGAT β-protein (41), which has been proposed to confer

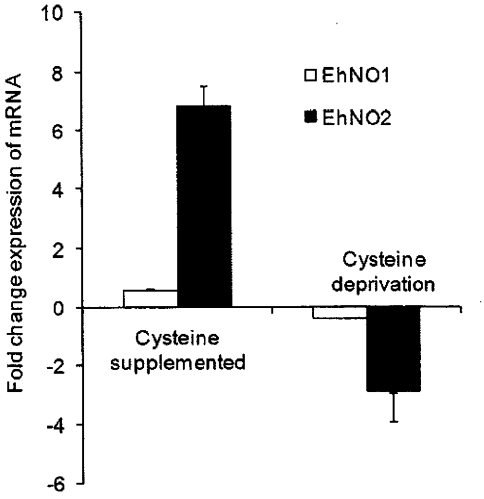

FIGURE 1. **Regulation of gene expression of EhNO isotypes in *E. histolytica* by extracellular L-cysteine concentration.** *E. histolytica* trophozoites were cultured in normal (8 mM), L-cysteine-supplemented (18 mM), or deprived medium. The expression levels of the EhNO transcripts under L-cysteine-supplemented or -deprived conditions were normalized against those of RNA polymerase II and are shown as the -fold change expression of mRNA relative to that of trophozoites from the control (normal) culture. *Error bars* represent the S.E. of three independent experiments.

specificity for NADPH, rather than NADH. The presence of alanine in place of glycine in the last residue of the motif G*X*G*XX*(G/A/P) (residues 269–274 of EhNO1 and 270–275 of EhNO2, shown in bold in supplemental Fig. S1) and a conserved arginine in the NAD(P)H binding domain (Arg-293 of EhNO1 and Arg-294 of EhNO2) (42) suggested that the two EhNOs prefer NADPH to NADH as a cofactor. Furthermore, a region in the carboxyl terminus (residues 401–411 of EhNO1 and 402–412 of EhNO2) matched the second FAD binding consensus sequence (TX_8GD).

Phylogenetic Analysis—Phylogenetic reconstruction was performed using neighbor-joining and maximum parsimony programs using 32 GOGAT β subunit or β subunit-like protein sequences from various organisms. The phylogenetic tree constructed using the neighbor-joining method revealed (supplemental Fig. S2) that EhNOs are more closely related to other β subunit-like homologs (supplemental Fig. S2, Group I) than to known GOGAT β subunit proteins (supplemental Fig. S2, Group II). This conclusion was also supported by the phylogenetic reconstruction using the maximum parsimony method (data not shown). Although these data did not clearly indicate the origin of the amebic GOGAT-like proteins, they suggested that EhNOs were most likely obtained by lateral gene transfer from an ancestral organism possessing a Group I-type gene, as reported previously for several other glutamate synthase β subunit-like genes (43).

Regulation of Gene Expression of EhNO Isotypes by L-Cysteine Concentration—To verify the transcriptomic data and confirm that the expression of EhNO1 and -2 was regulated by L-cysteine, the relative steady-state mRNA levels of the EhNO isotypes in *E. histolytica* trophozoites cultivated under L-cysteine-enriched or deprived conditions were measured by quantitative real-time PCR (Fig. 1). Using the RNA polymerase II 15-kDa subunit as an internal control, EhNO2 mRNA increased by

[4] A. Husain, D. Sato, G. Jeelani, M. Suematsu, T. Soga, and T. Nozaki, unpublished information.

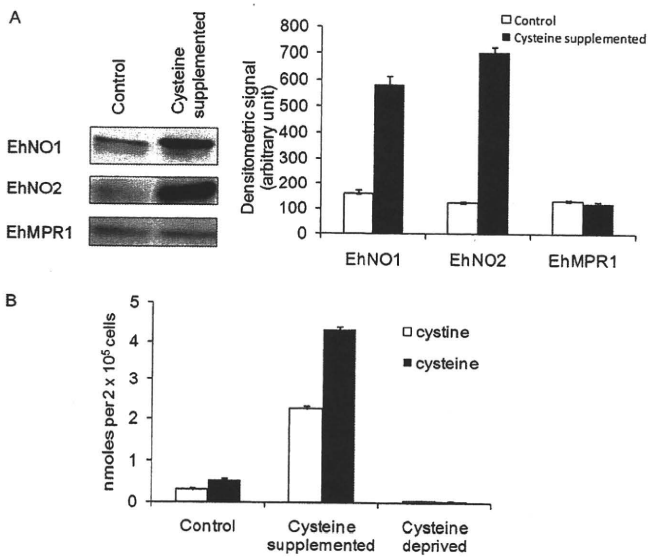

FIGURE 2. **Effects of extracellular L-cysteine concentrations on the amount of EhNO isotypes and intracellular L-cystine/L-cysteine concentrations.** *A*, an immunoblot analysis of EhNO1 and -2 is shown. After trophozoites were cultured under normal or L-cysteine-supplemented conditions for 48 h, ~15 μg of total cell lysate was electrophoresed on a 12% SDS-PAGE gel and subjected to an immunoblot assay with antibodies raised against EhNO1, EhNO2, or EhMPR1 as a control. The densitometric quantification of the reacted bands, shown in the *right graph*, was performed by Scion Image software, and the level of EhNO1, EhNO2, and EhMPR1 proteins was expressed in arbitrary units. *Error bars* represent the S.E. of three independent experiments. *B*, shown is intracellular L-cystine/cysteine concentrations under normal, L-cysteine-supplemented, and deprived conditions. L-Cystine/cysteine concentrations of the trophozoites cultivated for 48 h under the indicated conditions were analyzed by CE-MS. *Error bars* represent the S.E. of three independent experiments.

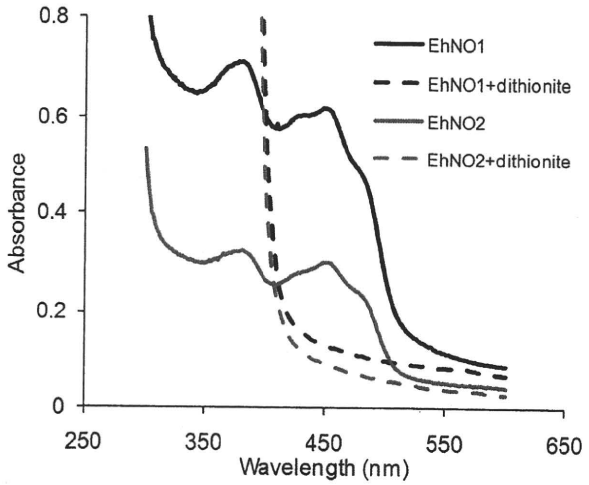

FIGURE 3. **Absorption spectra of rEhNO1 and rEhNO2 proteins.** UV-visible absorption spectra of rEhNO1 (400 μg of protein) and rEhNO2 (200 μg) under non-reducing (*solid lines*) and sodium dithionite-reducing conditions (*broken lines*) are shown. The samples were reduced with a 10-fold molar excess of sodium dithionite.

7-fold when cultured in the presence of 18 mM L-cysteine for 48 h compared with the control condition (8 mM L-cysteine), whereas it was down-regulated by 4-fold when cultured in the absence of L-cysteine. In contrast, the level of EhNO1 remained unchanged in either the presence or absence of L-cysteine.

Expression of EhNO Proteins under L-Cysteine-supplemented and -deprived Conditions—To confirm the changes of *EhNO* transcripts determined by the transcriptomic and real-time PCR analyses, we also examined EhNO expression at the protein level under L-cysteine-supplemented conditions. Immunoblot analysis using anti-rEhNO2 antibody showed that EhNO2 was induced by 6-fold when *E. histolytica* cultures were supplemented with L-cysteine (Fig. 2*A*). Although the RT-PCR results indicated that EhNO1 was not up-regulated under this condition, the protein recognized by anti-EhNO1 antibody was also found to be induced by 3.5-fold. Because anti-EhNO1 and anti-EhNO2 antibodies exhibited cross-reactivity (data not shown), the increased signal of the band recognized by anti-EhNO1 antibody was likely due to cross-reactivity with EhNO2. Alternatively, the level of EhNO1 may have increased by post-transcriptional mechanisms.

Changes in Intracellular L-Cysteine/Cystine Concentrations under L-Cysteine-supplemented and -deprived Conditions—To examine changes in intracellular L-cysteine and L-cystine concentrations caused by L-cysteine supplementation and deprivation, we quantitated their levels using a CE-MS-based approach in trophozoites maintained under normal (8 mM L-cysteine), enriched (18 mM L-cysteine), or deprived conditions. Under normal conditions, the L-cysteine to L-cystine ratio (1.70 ± 0.08) was deviated toward the reduced status. Upon L-cysteine supplementation, the intracellular levels of L-cysteine and L-cystine increased 8.1- and 7.3-fold, respectively, whereas under L-cysteine deprivation, both L-cysteine and L-cystine decreased to undetectable levels (Fig. 2*B*). Under L-cysteine-enriched conditions, the L-cysteine to L-cystine ratio (1.90 ± 0.14) slightly shifted toward the more reduced status (p = 0.031). Because several systems regulate the cellular redox reactions and electrochemical potential of the cell, the observed changes in the L-cysteine/cystine ratio were considered small. Taken together, these data clearly showed that although the extracellular L-cysteine concentration largely affects intracellular L-cysteine/L-cystine levels, its redox equilibrium is not severely affected. Furthermore, it appeared that a significant proportion of the L-cysteine incorporated into the cell was oxidized to L-cystine, which is supported by a previous finding (44). Alternatively, extracellular L-cysteine may be oxidized before uptake and reduced to L-cysteine intracellularly.

Expression and Purification of Recombinant EhNO Isotypes—To determine the biochemical properties of the two EhNO isoenzymes, recombinant proteins were first produced in *E. coli*. SDS-PAGE of the purified rEhNO1 and -2 proteins showed apparently single homogenous bands with molecular weights of 52.2 and 51.9 kDa, respectively, under reducing conditions (supplemental Fig. S3). The observed mobilities of rEhNO1 and -2 were consistent with the predicted sizes of the monomeric EhNO proteins with an extra 3.0-kDa histidine tag added at the amino terminus. The purity of the rEhNOs was estimated to be greater than 95% as judged by densitometric scanning of the stained gel. The rEhNO proteins were stable and retained their full activity for at least 3 months when stored in 10–15% glycerol at -30 or −80 °C.

Prosthetic Groups of rEhNOs—The UV-visible spectra of the purified rEhNOs showed absorbance maxima at 484, 450, 430, 378, and 280 nm (Fig. 3), which are characteristic of iron sulfur

flavoproteins (45). The dithionite-reduced rEhNOs showed, in contrast, a relatively featureless spectrum, with the increased absorbance at shorter wavelengths attributable to dithionite. Denaturation of the rEhNOs by boiling resulted in the release of flavin, indicating that it formed a non-covalent association with the protein. The fluorescence intensity of the free flavin at pH 2.6 was ~4-fold higher than that at pH 7.7 (data not shown). This indicates that FAD, rather than FMN, formed the prosthetic group in rEhNOs. It was calculated that 1.13 ± 0.32 mol of FAD (ϵ of FAD at 450 nm = 11.4×10^3 M^{-1} cm^{-1}) is associated per molecule of rEhNO1, whereas 0.89 ± 0.21 mol of FAD bound per molecule of rEhNO2. The iron analysis using the *O*-phenanthroline method indicated that rEhNO1 contained 7.8 ± 0.62 irons per molecule of rEhNO1, whereas rEhNO2 contained 7.4 ± 0.71 irons per molecule of rEhNO2. These results indicate that two [4Fe-4S] clusters are present per subunit, which is consistent with the $CX_2CX_4CX_3CP$ and $CX_3CX_3CX_3C$ motifs present in EhNO1 and -2. These data together with the stability of the enzymatic activity of rEhNOs also support the premise that rEhNOs retain most, if not all, of the features of the native EhNOs.

Kinetics Properties of rEhNO—The rEhNOs were devoid of glutamate synthase and glutamate dehydrogenase activity in both directions at either pH 7.5 or 9.5. However, both proteins oxidized NADPH and transferred electrons to several alternative electron acceptors, including INT, ferricyanide, and menadione (Table 1). In the presence of NADPH, the reduction rate of INT by rEhNO1 (specific activity 19.42 ± 3.25 μmol min^{-1} mg^{-1}) was >30-fold higher than that by rEhNO2 (0.62 ± 0.10 μmol min^{-1} mg^{-1}), whereas rEhNO2 showed a 2.8-fold higher ferricyanide reducing activity (86.64 ± 8.33 μmol min^{-1} mg^{-1}) than rEhNO1 (31.50 ± 6.21 μmol min^{-1} mg^{-1}). The menadione-reducing activities of rEhNO1 and -2 were comparable (2.48 ± 0.39 and 2.25 ± 0.41 μmol min^{-1} mg^{-1}, respectively). Both rEhNO1 and -2 were highly specific toward NADPH and did not reduce the above-tested electron acceptors with NADH as the electron donor. In the NADPH:flavin oxidoreductase reaction under aerobic conditions, rEhNO1 and -2 produced H_2O_2 at comparable levels (Table 1). Significantly, the two enzymes were also capable of reducing the anti-amebic drug metronidazole and the herbicide paraquat.

In addition to these properties, rEhNO1 and -2 could catalyze the reduction of disulfides, such as L-cystine, which was also dependent on NADPH. The K_m and k_{cat}/K_m values of rEhNO1 and -2 for L-cystine and NADPH were significantly different (Table 2). At substrate-saturating concentrations, the K_m values of rEhNO1 for L-cystine and L-NADPH were 3.3- and 2.3-fold higher, respectively, than those of rEhNO2. The k_{cat}/K_m value of rEhNO2 for L-cystine (measured at saturating concentrations of NADPH) was ~4-fold higher than that of rEhNO1. The addition of *N*-ethylmaleimide, which is commonly used to inhibit sulfydryl-dependent reactions, inhibited the disulfide reducing activities of both rEhNO1 and rEhNO2 (0.5 mM *N*-ethylmaleimide caused 50% inhibition), whereas the presence of up to 5 mM *N*-ethylmaleimide had no effect on the reduction of INT. These results indicate that the two EhNOs contain thiol(s) groups that are involved in disulfide reduction but are not required for their observed oxidoreductase activity (46, 47).

We also found that rEhNO1 and -2 catalyzed the reduction of ferric to ferrous ion. In the presence of NADPH, the reduction rate of Fe(III) by rEhNO1 (k_{cat}/K_m 15.1 ± 3.20 min^{-1} μM^{-1}) was ~116-fold higher than that by rEhNO2 (k_{cat}/K_m 0.12 ± 0.01 min^{-1} μM^{-1}) (Table 2). In addition, both rEhNOs also acted as ferredoxin:$NADP^+$ reductases capable of catalyzing the reduction of $NADP^+$ to NADPH through the utilization of the electrons provided by reduced ferredoxin, although the observed activity of EhNO1 was again higher (7.8-fold) than that of EhNO2. These data suggest that EhNO1 is mainly involved in the reduction of ferric ion and ferrodoxin:$NADP^+$, whereas EhNO2 primarily catalyzes the reduction of L-cystine. The uncatalyzed reaction rate (without enzyme) of each reaction was as follows: 22.5 ± 2.4 pmol/min, INT; 250 ± 32 pmol/min, ferricyanide; 29.2 ± 6.1 pmol/min, menadione; 307 ± 66 pmol/min, paraquat; 22.5 ± 7.8 pmol/min, cystine; 28.9 ± 6.9 pmol/min, ferric ammonium citrate; 6.16 ± 2.7 pmol/min, ferredoxin.

Binary Complexes of EhNO1/2 with Ferredoxins—To examine whether electron transfer between reduced ferredoxin and $NADP^+$ by EhNO1 was dependent on the physical interaction between these two proteins (48), as reported for the spinach leaf redox couple (36), we investigated whether EhNO1 and -2

TABLE 1

Specific activity of purified EhNO1 and EhNO2 with various electron acceptors

Values are expressed as the means ± S.D. of three independent experiments as described under "Experimental Procedures"

Substrate	Specific activity	
	rEhNO1	rEhNO2
	μmol/min/mg	
INT	19.42 ± 3.25	0.62 ± 0.10
Ferricyanide	31.50 ± 6.21	86.64 ± 8.33
Menadione	2.48 ± 0.39	2.25 ± 0.41
Metronidazole	1.75 ± 0.42	1.41 ± 0.46
Paraquat	19.73 ± 4.23	10.60 ± 2.12
Oxygen	8.31 ± 2.12	3.42 ± 0.81

TABLE 2

Kinetic parameters for cystine, ferric, and ferredoxin $NADP^+$ reductase reactions catalyzed by EhNO1 and EhNO2

Values are expressed as the means ± S.D. of three independent experiments.

Substrate	rEhNO1				rEhNO2			
	K_m	V_{max}	k_{cat}	k_{cat}/K_m	K_m	V_{max}	k_{cat}	k_{cat}/K_m
	μM	*μmol/min/mg*	min^{-1}	$min^{-1} \cdot \mu M^{-1}$	*μM*	*μmol/min/mg*	min^{-1}	$min^{-1} \cdot \mu M^{-1}$
Cystine	910 ± 20	0.88 ± 0.06	45.86 ± 7.52	0.05 ± 0.01	276 ± 23	1.15 ± 0.17	59.36 ± 3.81	0.22 ± 0.13
NADPH (cystine)	9.2 ± 2.1	1.70 ± 0.13	88.38 ± 5.83	9.61 ± 1.34	4.2 ± 0.8	1.33 ± 0.43	68.62 ± 5.40	16.33 ± 2.12
Fe(III) citrate	31.3 ± 3.4	9.10 ± 2.51	471.2 ± 17.5	15.1 ± 3.20	98.4 ± 4.5	0.26 ± 0.09	12.18 ± 2.81	0.12 ± 0.01
NADPH (ferric)	70.3 ± 4.9	10.12 ± 3.16	526.6 ± 21.2	7.49 ± 2.12	66.7 ± 8.3	0.72 ± 0.31	37.06 ± 6.28	0.56 ± 0.23
Ferredoxin	0.16 ± 0.05	2.28 ± 0.46	118.8 ± 7.4	742.5 ± 34.1	0.23 ± 0.07	0.43 ± 0.18	21.71 ± 4.51	94.39 ± 8.91